

NACA TN 2904

# NATIONAL ADVISORY COMMITTEE FOR AERONAUTICS

TECHNICAL NOTE 2904

IMPINGEMENT OF WATER DROPLETS ON A CYLINDER IN AN  
INCOMPRESSIBLE FLOW FIELD AND EVALUATION OF ROTATING  
MULTICYLINDER METHOD FOR MEASUREMENT OF  
DROPLET-SIZE DISTRIBUTION, VOLUME-MEDIAN  
DROPLET SIZE, AND LIQUID-WATER CONTENT  
IN CLOUDS

By Rinaldo J. Brun and Harry W. Mergler

Lewis Flight Propulsion Laboratory  
Cleveland, Ohio



Washington  
March 1953

NATIONAL ADVISORY COMMITTEE FOR AERONAUTICS

---

TECHNICAL NOTE 2904

---

IMPINGEMENT OF WATER DROPLETS ON A CYLINDER IN AN INCOMPRESSIBLE FLOW  
FIELD AND EVALUATION OF ROTATING MULTICYLINDER METHOD FOR  
MEASUREMENT OF DROPLET-SIZE DISTRIBUTION, VOLUME-MEDIAN  
DROPLET SIZE, AND LIQUID-WATER CONTENT IN CLOUDS

By Rinaldo J. Brun and Harry W. Mergler

SUMMARY

Evaluation of the rotating multicylinder method for the measurement of droplet-size distribution, volume-median droplet size, and liquid-water content in clouds showed that small uncertainties in the basic data eliminate the distinction between different cloud droplet-size distributions and are a source of large errors in the determination of the droplet size. Calculations of the trajectories of cloud droplets in an incompressible-air flow field around a cylinder were performed on a mechanical analog constructed for the study of the trajectories of droplets around aerodynamic bodies. Many data points were carefully calculated in order to determine precisely the rate of droplet impingement on the surface of a right circular cylinder.

Matching curves for obtaining droplet-size distribution, volume-median droplet size, and liquid-water content from flight data were computed from the results of the droplet-trajectory calculations. An evaluation is presented of the rotating multicylinder method for the measurement of droplet-size distribution, volume-median droplet size, and liquid-water content in clouds. Because of the insensitivity of the multicylinder method to changes in conditions in clouds, and the inaccuracies in obtaining flight data, errors as large as 70 percent in the determination of the volume-median droplet size are possible if the flight speed is 200 miles per hour and the actual volume-median droplet diameter in the cloud is 30 microns.

INTRODUCTION

As part of a comprehensive aircraft ice-protection research program, the NACA has undertaken an investigation of the impingement of water droplets on aerodynamic bodies. Previous investigators have calculated

the water-droplet trajectories for right circular cylinders (references 1 to 5) and for airfoils (references 6 to 8). The trajectory results on airfoils have been applied to the design of equipment for the protection of aircraft components against ice formation. The calculations of water-droplet impingement on cylinders have occasionally been used for the same purpose but are most useful in connection with flight instruments used in the study of droplet size and distributions in icing clouds.

A commonly used technique for measuring the liquid-water content and droplet-size distribution in icing clouds is described in reference 9 as the rotating multicylinder method. Several right circular cylinders of different diameters are exposed from an airplane in flight to the supercooled droplets in a cloud, as shown in figure 1. An assembled set of rotating multicylinders is shown in figure 2. In the usual procedure for obtaining the cloud-droplet data, the multicylinders are extended through the airplane fuselage during the exposure run and then are retracted for disassembling and weighing. It is assumed that all those supercooled droplets that strike the cylinders freeze completely on the cylinders. The liquid-water content and droplet-size distribution are determined by a comparison of the measured weight of ice collected on each of the cylinders with the droplet-impingement results obtained from calculated water-droplet trajectories for the same cylinders.

The mechanical operation of the rotating multicylinder method is reliable, because it lacks technical complexity and is adaptable to flight use. The meteorological data obtained with the multicylinder method have been the only data available in the design of ice-protection equipment for aircraft. An important disadvantage of the method lies in its insensitivity in discriminating among the different droplet-size distributions.

Trajectories of droplets in a compressible-air flow field around a cylinder were calculated (reference 4) in order to evaluate the effect of the compressibility of air on the trajectories of cloud droplets. Trajectories in an incompressible flow field were also calculated during the investigation reported in reference 4 for comparison with those obtained in a compressible-air flow field. Some difference was found between the trajectories in the incompressible flow field and the results presented in references 1 to 3, in which the trajectories were also calculated for an incompressible flow field around a cylinder. Also, a considerable difference was found to exist among the references cited. Because of the differences in the existing literature, a recalculation of the trajectories in an incompressible flow field around a cylinder was undertaken at the NACA Lewis laboratory.

In reference 1 the forces acting on the water droplet were calculated from Stokes' law for slow translatory motion of a small sphere in an incompressible viscous fluid. The forces acting on the water droplet were calculated more precisely in reference 3 by the use of the experimentally determined drag coefficient for a sphere in terms of the Reynolds number. The calculations for the trajectories were performed in reference 1 by a step-by-step integration of the second-order non-linear differential equations that describe the motion of the droplets around a cylinder. The calculations presented in reference 3 were made more accurately with the use of a differential analyzer.

The method used in reference 3 for calculating the water-droplet trajectories has been used for calculating the data presented herein. Many more data points were carefully calculated for the results presented herein than were calculated for the data in reference 3, in order to determine more precisely the rate of impingement of droplets on the surface of the cylinder. Accuracy was emphasized in all the calculations, because the sensitivity of the rotating multicylinder method in its application does not permit wide tolerances in the theoretical data. Curves were established over a wide range of the variables in order to determine whether the impingement on cylinders follows rules that might be available for extension in future studies to other aerodynamic bodies.

#### SYMBOLS

The following symbols are used in this report:

- a droplet radius, ft ( $3.048 \times 10^5$  microns)
- $C_D$  drag coefficient for droplets in air, dimensionless
- D drag force, lb
- d droplet diameter, microns ( $3.28 \times 10^{-6}$  ft)
- E collection efficiency based on cylinder radius, dimensionless
- K inertia parameter,  $\frac{2}{9} \frac{\rho_w a^2 U}{\mu L}$ , dimensionless
- L cylinder radius, ft
- Re local Reynolds number with respect to droplet,  $2a\rho_a \bar{v}/\mu$ , dimensionless
- $Re_0$  free-stream Reynolds number with respect to droplet,  $2a\rho_a U/\mu$ , dimensionless
- t time, sec

- U free-stream velocity, ft/sec
- u local air velocity, ratio of the actual local air velocity to the free-stream velocity, dimensionless
- v local droplet velocity, ratio of the actual droplet velocity to the free-stream velocity, dimensionless
- $\bar{v}$  local vector difference between velocity of droplet and velocity of air, ft/sec
- W rate of water collection per unit span of cylinder, slugs/(sec)(ft span)
- $W_{\beta}$  local rate of water impingement, slugs/(sec)(sq ft)
- w liquid-water content in the atmosphere, slugs/cu ft
- x,y rectangular coordinates, ratio of actual distance to cylinder radius L, dimensionless
- $\beta$  local impingement efficiency,  $dy_0/d\theta$ , dimensionless
- $\theta$  impingement angle on cylinder, deg or radians as noted
- $\mu$  viscosity of air, slugs/(ft)(sec)
- $\rho$  density, slugs/cu ft
- $\tau$  time scale,  $tU/L$ , dimensionless
- $\varphi \frac{Re_0^2}{K} \equiv \frac{18\rho_a^2 LU}{\mu\rho_w}$ , dimensionless

## Subscripts:

- a air
- m maximum
- o volume median
- w water
- x horizontal component
- y vertical component

$\omega$  weighted

0 free-stream condition

Prime superscript applied where velocity terms are in ft/sec

## ANALYSIS

### Derivation of Equations of Motion

As a cylinder moves through a cloud, the amount of water intercepted by the cylinder is dependent on the inertia of the cloud droplets. In order to obtain the extent of impingement and the rate of droplet impingement per unit area on a cylinder, the cloud-droplet trajectories with respect to the cylinder must be determined. The differential equations that describe the droplet motion have been stated in reference 3 and are derived in the following paragraphs.

From the conventional forms of the equations for the drag force of a body in a fluid

$$D = C_D \frac{1}{2} \rho_a \pi a^2 \bar{v}^2$$

and for Reynolds number

$$Re = \frac{2a\rho_a\bar{v}}{\mu}$$

there is obtained

$$D = \frac{C_D Re}{4} \pi a \mu \bar{v}$$

for a sphere having a relative velocity  $\bar{v}$  with respect to the fluid. The equation of motion of a water droplet in terms of its  $x$ -component in a rectangular coordinate system is

$$\frac{4}{3} \pi a^3 \rho_w \frac{dv'_x}{dt} = \frac{C_D Re}{4} \pi a \mu (u'_x - v'_x)$$

$$\left( \frac{2}{9} \frac{a^2 \rho_w U}{\mu L} \right) \frac{dv'_x}{dt} \frac{L}{U^2} = \frac{C_D Re}{24} \frac{(u'_x - v'_x)}{U}$$

where the velocity terms with the prime superscript have the dimensions of feet per second. In dimensionless terms the equation of motion for the x-component becomes

$$\frac{dv'_x}{d\tau} = \frac{C_D Re}{24} \frac{1}{K} (u_x - v_x) \quad (1)$$

and for the y-component becomes

$$\frac{dv'_y}{d\tau} = \frac{C_D Re}{24} \frac{1}{K} (u_y - v_y) \quad (2)$$

where

$$K \equiv \frac{2}{9} \frac{\rho_w a^2 U}{\mu L} \quad (3)$$

The Reynolds number  $Re$  can be obtained conveniently in terms of the free-stream Reynolds number

$$Re_0 = \frac{2a\rho_a U}{\mu} \quad (4)$$

such that

$$\left(\frac{Re}{Re_0}\right)^2 = (u_x - v_x)^2 + (u_y - v_y)^2 \quad (5)$$

The term  $C_D Re/24$  containing the coefficient of drag for the droplets, required in equations (1) and (2), may be obtained from tables in references 3 or 6. The values presented in references 3 or 6 were obtained from experimental wind-tunnel data on the drag forces on spheres, presented in reference 10. As the relative motion between the droplets and air approaches zero as a limiting value, the value of  $C_D Re/24$  approaches unity as the limiting value, and Stokes' law for the drag forces acting on the water droplets applies.

The air velocity components (reference 11) for a cylinder in a uniform, potential, and incompressible flow in two dimensions and without circulation are

$$\left. \begin{aligned} u_x &= 1 + \frac{y^2 - x^2}{(x^2 + y^2)^2} \\ u_y &= -\frac{2xy}{(x^2 + y^2)^2} \end{aligned} \right\} \quad (6)$$

Equations (1) to (6) are written in dimensionless form in order to maintain the number of calculations at a minimum and to simplify the presentation of the results. The equations apply to the motion of droplets in a plane perpendicular to the axis of the cylinder, which is located at the origin of the rectangular coordinate system, as shown in figure 3. At an infinite distance ahead of the cylinder, the uniform air flow carrying the cloud droplets is assumed to be approaching the cylinder from the negative x-direction and parallel to the x-axis. All the distances appearing in the equations and in the figures are ratios to the cylinder radius  $L$ , which is assumed to be the unit of distance. The velocities appear as fractional parts of the free-stream velocity  $U$ . Time is expressed in terms of the cylinder radius and free-stream velocity, such that

$$\tau = \frac{tU}{L}$$

In this manner the unit of time is the time required for a droplet to travel a distance  $L$  at velocity  $U$ . The Reynolds number is expressed with respect to the droplet radius.

The differential equations (1) and (2) state that the motion of a droplet is governed by the drag forces imposed on the droplet by the relative motion between the droplet and the air moving along the streamlines around the cylinder. The droplet momentum tends to keep the droplet moving in a straight path, while the drag forces tend to force the droplet to follow the streamlines. For very small droplets and slow speed, the momentum of the droplets parallel to the direction of the free-stream motion is small, and the drag forces are large enough that little deviation from the streamlines occurs; whereas, for large droplets or high speed, the momentum is large enough to cause the droplets to deviate from the streamlines. In accordance with the statement of equations (1) and (2) and the definition of the parameter  $K$  in equation (3), the trajectories depend on the size of the cylinder, the radius of the droplet, the airspeed and the air viscosity as first-order variables.

The more important assumptions that have been necessary in order to solve the problems are:

- (1) At a large distance ahead of the cylinder (free-stream conditions) the droplets move with the same velocity as the air.
- (2) The droplets are always spherical and do not change in size.
- (3) No gravitational force acts on the droplets.



### Method of Calculation

The differential equations of motion (equations (1) and (2)) are difficult to solve by ordinary means because the actual values of the velocity components of the droplet relative to the air and the term containing the coefficient of drag are not known until the trajectory is traced. These values are determined as the trajectory of a droplet is developed, because their magnitude depends on the position of the droplet in the flow field. Simultaneous solutions for the two equations of motion were obtained with the use of a mechanical analog based on the principle of a differential analyzer. A description of this analog and the method of solution for the droplet trajectories are presented in appendix A. The answers were obtained in the form of plots of the droplet trajectories with respect to the cylinder, as shown in figure 4. The second quadrant section of the cylinder is outlined. The ordinate scale was expanded approximately four times the abscissa scale with appropriate gearing in the analog (appendix A) in an effort to obtain the maximum accuracy in the determination of the points of impingement of the droplets on the cylinder surface.

Before the integration of the equations of motion could be performed with the analog, the velocity of the droplets at the start of the integration had to be determined. As has been postulated in the assumptions, at an infinite distance ahead of the cylinder, all the droplets have vertical and horizontal components of velocity that are the same as those of the free-stream air. At finite distances ahead of the cylinder, the droplets have velocity components and positions varying between those pertaining to the undisturbed free stream and those pertaining to the air streamlines. A study of the air streamlines showed that only a gradual deviation of the air streamlines from the free-stream velocity takes place up to approximately 5 radii ahead of the cylinder center line. A large rate of change of air motion takes place between  $x = -5$  and the cylinder surface. The equations of motion (equations (1) and (2)) were linearized by an approximation and solved between  $x = -\infty$  and  $x = -5$  by the method presented in reference 3 and discussed herein in appendix B. The trajectories of the droplets impinging on the cylinder are shown in figure 4 plotted from  $x = -5$  to the point of impingement on the cylinder surface. The analog starting conditions at  $x = -5$ , as calculated by the linearized equations, were estimated to be as accurate as the expected accuracy of the analog (appendix B).

The trajectories shown in figure 4 are representative of operating conditions which result in values of  $K = 4$  and  $Re_0 = 63.246$  (equations (3) and (4)). The topmost trajectory (A) is tangent to the cylinder and determines the maximum extent of impingement of droplets for the conditions given for figure 4. All droplets having trajectories below this tangent trajectory strike the cylinder; whereas, all droplets having trajectories above this line will miss the cylinder.

The impingement of droplets on the third quadrant of the cylinder (fig. 3) is identical to the impingement on the second quadrant, except that the trajectories are mirror images of the trajectories shown in figure 4. The amount of water impinging on the cylinder is the total water in those droplets bounded by the second-quadrant tangent trajectory and the third-quadrant tangent trajectory. If the cloud of droplets is assumed to be uniform at a large distance ahead of the cylinder (free-stream conditions), the water intercepted by the cylinder per unit time is the water contained in a volume of cloud of unit depth and length but with a width that has twice the value of  $y_{0,m}$ , the ordinate at infinity of the tangent trajectory.

For the conditions of  $K$  and  $Re_0$  applicable to the trajectories shown in figure 4, the tangent trajectory (A) also determines the cylinder collection efficiency, which is defined as the ratio of the actual water in the droplets intercepted by the cylinder to the total water in the volume swept out of its path by the cylinder. For a cloud composed of droplets all uniform in size the collection efficiency is equal to  $y_{0,m}$  in magnitude, because in the trajectory calculations the ordinate  $y_{0,m}$  is given as a ratio to the cylinder radius.

The tangent trajectories were computed in order to obtain the water intercepted by the cylinder and the cylinder collection efficiency. The trajectories intermediate between the  $x$ -axis and the tangent trajectory were computed in order to obtain the distribution of the water on the cylinder surface. The tangent trajectories also determine the angle of maximum extent of impingement. The angle of maximum extent of impingement is denoted by  $\theta_m$  (fig. 4), and the angle of impingement of the intermediate trajectories is denoted by  $\theta$ . The accuracy in determining  $\theta_m$  was approximately  $\pm 1.5^\circ$ .

Trajectories for droplets with low inertia hovered along the surface of the cylinder over large circumferential distances. The crowding together of the trajectories near the cylinder for very low values of  $K$  did not permit the  $\pm 1.5^\circ$  accuracy to be maintained for values of  $K < 1$  with the same scale factors shown in figure 4. For values of  $K < 1$  the scale factors of the cylinder were increased such that the trajectories were plotted with respect to a cylinder 40 inches in diameter. For these low values of  $K$  the ordinate scale was not distorted with respect to the abscissa scale. A small section of the cylinder surface with the trajectories of droplets impinging on it is shown in figure 5. Although only the portion of the trajectories from  $x = -2$  up to the cylinder surface is shown in figure 5, the trajectories were calculated by the machine from  $x = -5$  and the starting conditions at  $x = -5$  were obtained as explained in appendix B. An attempt was made to increase the ease in locating the point of tangency by calculating a trajectory slightly below the tangent trajectory and running the trajectory through

the cylinder (trajectories B, fig. 5). The trajectory near the tangent trajectory defined the tangency by cutting the cylinder at two definite points, such as a secant line. This method of determining the tangent is accurate only if trajectory B is very near the tangent trajectory. The increase in scale factor permitted an accuracy of  $\pm 1.5^\circ$  to be obtained for  $\theta_m$  for  $K = 0.5$ , and  $\pm 2^\circ$  for  $K = 0.25$ .

#### Method of Presenting Data

Series of trajectories, such as those shown in figure 4, computed for several combinations of values of  $K$  and  $Re_0$ , permit the evaluation of area, rate, and distribution of water-droplet impingement on cylinders. The data are presented herein in terms of dimensionless parameters in order to generalize the presentation of the data and to gain in flexibility in the application of the data to experimental and analytical studies. Examples involving dimensions and flight conditions are used herein whenever the examples are aids in clarifying the presentation of the data. Typical values of dimensions and flight conditions are used in most of the examples given; however, because of the nature of the dimensionless parameters, a large number of combinations of values of the variables, such as free-stream velocity, cylinder size, droplet size, and others (equations (3) and (4)), would apply to the particular value of the dimensionless parameter illustrated by the example. A system of equations for the evaluation of dimensionless parameters in terms of variables with units commonly employed in aeronautics is presented in appendix C.

The results are often presented herein as functions of the parameter  $K$ . The parameter  $K$  has been termed the inertia parameter, because its magnitude directly reflects the external force required on a droplet to cause a deviation from the original line of motion of the droplet. A dimensionless parameter  $\Phi$ , defined as

$$\Phi \equiv \frac{Re_0^2}{K} = \frac{18\rho_a^2LU}{\mu\rho_w} \quad (7)$$

was adopted in reference 3 for the presentation of the data and is also employed herein. The parameter  $\Phi$  is valuable in that  $\Phi$  is not a function of droplet size. The parameter  $\Phi$  is an important concept in the interpretation of icing-cloud measurements in which the droplet size is not measured directly and is an unknown which must be calculated (appendix D). In the interpretation of icing-cloud measurements in which cylinders of different diameters are exposed to the supercooled droplets from an airplane in flight,  $\Phi$  may be considered to be a function of altitude through its dependence on air density  $\rho_a$  and viscosity  $\mu$  for each cylinder size and a given flight speed.

The magnitude of  $\varphi$  is a measure of the deviation from Stokes' law for the forces acting on the water droplets. Stokes' law was derived for slow translatory motion of a small sphere in an incompressible viscous fluid and applies precisely in the limiting value of  $\varphi = 0$ , when the free-stream Reynolds number is zero or the droplet motion relative to the cylinder approaches zero as the limit (equation (7)).

## RESULTS AND DISCUSSION

Collection efficiency. - The collection efficiency as a function of the inertia parameter  $K$  and the parameter  $\varphi$  is presented in figure 6. For the conditions in which a cylinder is moving through a cloud of droplets that are all uniform in size, the total rate of water interception per foot span of the cylinder is

$$W_m = 2E_m L U w \quad (8)$$

The collection efficiency increases with increasing values of  $K$ . The primary variables in the inertia parameter  $K$  (equation (3)) are the droplet size, the free-stream velocity, and the cylinder size. The range of variation of water density or air viscosity over the range of temperature changes in the ordinary atmosphere from sea level to 30,000 feet is small compared with the range of variation possible with the other variables in equation (3).

The collection efficiency increases with increasing droplet size and free-stream velocity, because an increase in the free-stream momentum of the droplet with respect to a cylinder increases the forces necessary to force the droplet around the cylinder. An increase in the cylinder size decreases the collection efficiency, because the large cylinders cause the air streamlines to start moving around the cylinder a greater actual distance (not in terms of ratio to cylinder radius) ahead of the cylinder than the small cylinders. The greater distance ahead of the cylinder in which the streamlines are moving around the large cylinder permits the air drag forces to act on the droplets for a long time  $t$  in seconds, thus causing a smaller portion of the droplets that are in the path of the cylinder to impinge on the cylinder.

For the conditions in which Stokes' law applies for the drag force ( $\varphi = 0$ ), the values of figure 6 for collection efficiency are very nearly the same as those presented in reference 3. The results of figure 6 and reference 3 are both lower than those presented in references 1 and 2, again for  $\varphi = 0$ . The calculations for the work presented in references 1 and 2 were not made with differential analyzers, nor were the conditions at the start of the trajectories determined by the method presented in appendix B. The differences may result from either the

method of calculation or the assumptions at the starting conditions. The calculations of reference 2 included only values of  $K$  less than 2. The results of figure 6 differ somewhat with those of reference 3. For  $\varphi = 10,000$ , the results of figure 6 are higher than those in reference 3 by 0, 8, 7, 2, and 0 percent for  $K = 1, 4, 16, 36,$  and 256, respectively. The calculated points shown in figure 6 are presented in table I. Corresponding points obtained from curves given in reference 3 are also given in table I for comparison. No calculations were made in references 1 and 2 for values of  $\varphi$  other than zero. Although a few calculations were made in reference 5 for  $\varphi = 16,000$ , the results are not comparable with either the results presented herein or in reference 3, because the starting conditions and method of computation were not the same.

The expanded ordinate scale used with the analog permitted the calculations presented herein for the collection efficiency to be read accurately within  $\pm 0.002$  unit for values of  $E_m$  between 0.20 and 1.00. The accuracy in obtaining  $E_m$  for values of  $K = 0.5$  and 0.25 was  $\pm 0.003$  and  $\pm 0.004$ , respectively, because the accuracy in the determination of the tangent trajectory was not as good for the low values of  $K$ , as was stated in a previous section. The values shown in figure 6 for  $K = 0.5$  and 0.25 are averages of two or more check calculations.

Maximum angle of impingement. - The maximum angle of impingement is given in figure 7 as a function of  $K$  and  $\varphi$ . The maximum angle of impingement, in radians, increases with increasing values of the inertia parameter. The shapes of the curves in figure 7 are similar to those in figure 6 on the collection efficiency. As was discussed in the section titled Method of Calculation, the accuracy in determining  $\theta_m$  was  $\pm 1.5^\circ$  for conditions in which  $K = 0.5$ . The curves of figure 7 were faired through averages of readings by several observers of the original trajectory plots. In the low values of  $K$  ( $K < 1$ ) two or often more than two check analog calculations were made. A comparison of the angle of impingement given by the curves of figure 7 with the results of reference 3 is made in table I.

Tangential-velocity components. - The tangential-velocity components of both the air and those droplets that are tangent to the surface of the cylinder are presented in figure 8 in the form of a velocity hodograph. The vertical and horizontal components of the air velocity at the surface of the cylinder can be found from the outermost velocity hodograph. The graduations denote the angle  $\theta$  measured clockwise on the cylinder from the  $-x$  ordinate to the  $+y$  ordinate (fig. 3). The velocity components of those droplets that impinge tangentially to the cylinder (trajectory A, fig. 4) can be found from the hodograph enclosed by the air hodograph. A line passing through the 0,0 ordinates of the hodograph and a given position angle  $\theta$  on the air hodograph will give the velocity direction of both the air and the droplets at that point on the cylinder, because

both the air and the droplet velocities are tangent to the cylinder. The values of the inertia parameter  $K$  that correspond to the calculated points are shown at each point. Apparently, the velocity components for all droplets, regardless of the combination of  $\phi$  and  $K$ , can be represented by one curve. This relation between  $v_y$  and  $v_x$  was also noted for airfoils in reference 7.

The method for obtaining the vertical and horizontal component velocities of both the air and the droplets is illustrated for the example involving a cylinder  $1\frac{5}{8}$  inches in diameter moving with a free-stream velocity of 125 miles per hour at 10,000 feet NACA standard altitude conditions through a cloud composed of uniform droplets 20 microns in diameter. For these conditions  $K = 3.6$  and  $\phi = 1000$ . The maximum angle of impingement, which corresponds to the point on the cylinder where these droplets impinge tangentially, is found in figure 7 to be 1.172 radians or  $67^\circ$ . The vertical component of droplet velocity  $v_y$  at the point of tangency on the cylinder is 0.41 and the horizontal component  $v_x$  is 0.96, both values being given in figure 8 as ratios to the free-stream velocity. The air velocity components  $u_y$  and  $u_x$  are 0.72 and 1.69, respectively, times the free-stream velocity.

At the cylinder angle  $\theta_m$  of  $90^\circ$ , all the horizontal droplet velocities must be unity, which is the free-stream velocity, because only the droplets with infinite inertia will be tangent to the  $90^\circ$  point on the cylinder.

Impingement of intermediate trajectories. - The starting ordinate  $y_0$  at infinity of any trajectory, including the trajectories between the tangent trajectory and the  $x$ -axis such as shown in figure 4, can be found in figure 9 for any given angle of impingement on the cylinder. The starting and ending positions of the trajectories are shown in figure 9 for the five different values of  $\phi$  studied. For each value of  $\phi$ , curves for several values of  $K$  are presented. The choice of the particular values of  $K$ , shown in each figure, was governed by the gearing available for the analog.

The amount of water impinging between any two given points on a cylinder moving through a uniform cloud can be found from the results given in figure 9. For example, if the amount of water impinging between the  $x$ -axis and a point  $\theta = 45^\circ = 0.785$  radian must be known for a  $\frac{1}{2}$ -inch cylinder moving with a free-stream velocity of 130 miles per hour through a cloud composed of 20-micron droplets, the value of  $y_0$  to be used in the relation

$$W = U_w L y_0 \quad (9)$$

can be found in figure 9(c) for  $\varphi = 1000$  and  $K = 4$ . The value of  $y_0$  is found to be 0.53 and is the value used in equation (9). The amount of water impinging between two points, where one of the points is not on the x-axis, is found by using the relation

$$W = UwL (y_{0,2} - y_{0,1}) \quad (9a)$$

The angle  $\theta$  is given in radians in figure 9 because radians permit a convenient conversion of the data of figure 9 in the determination of local rates of water impingement discussed in a subsequent section.

An analysis of the data points shown in figure 9 reveals that all the points fell on sine curves, with amplitude and period depending on the values of  $K$  and  $\varphi$  studied. The reason for this behavior is not apparent from a study of the equations of motion (equations (1) and (2)), which are very nonlinear and do not permit a formal solution. However, this behavior of the data can be used advantageously in that curves of  $y_0$  as a function of  $\theta$  for values of  $\varphi$  and  $K$  in addition to those curves given in figure 9 are possible with the aid of the expression

$$y_0 = E_m \sin \left( \frac{\pi}{2} \frac{\theta}{\theta_m} \right) \quad (10)$$

The following examples illustrate the use of equation (10). If the curve of  $y_0$  as a function of  $\theta$  for  $\varphi = 100$  and  $K = 2$  is desired (shown in fig. 9(b) without calculated points), the amplitude and period that determine the terminus of the desired curve are obtained from figures 6 and 7, respectively. The value of  $y_{0,m} = E_m = 0.493$  is found in figure 6, and the value of  $\theta_m = 1.092$  is found in figure 7. These values of  $y_{0,m}$  and  $\theta_m$  are the terminus values and a measure of the amplitude and period, respectively, of the desired sine curve for  $\varphi = 100$  and  $K = 2$ . Other points along the desired curve are obtained by solving equation (10) over a range of values of  $\theta$  from 0 to  $\theta_m$ .

If a knowledge is required of the amount of water impinging between  $\theta = 40^\circ = 0.698$  radian and  $\theta = 50^\circ = 0.873$  radian on a cylinder for which the operating conditions were  $K = 6$  and  $\varphi = 3000$ , the value of  $(y_{0,2} - y_{0,1})$  required in equation (9a) is found by the interpolation of the curves presented in figures 6 and 7. The value of  $y_{0,m} = E_m$  is found from figure 6 to be 0.66. The value of  $\theta_m$  is found from figure 7 to be 1.255. The values of  $\theta/\theta_m$  required for use with equation (10) are  $0.698/1.255 = 0.556$  and  $0.873/1.255 = 0.696$  for the

two points of interest on the cylinder. The value of  $(y_{0,2} - y_{0,1})$  for use in equation (9a) is

$$0.66 \left[ \sin \left( \frac{\pi}{2} 0.696 \right) - \sin \left( \frac{\pi}{2} 0.556 \right) \right] = 0.080$$

The dashed lines in figure 9 are the loci of the termini of the sine curves. These dashed lines are cross plots of the curves given in figures 6 and 7. The accuracy in determining the dashed lines is the same as the accuracy for figures 6 and 7. The accuracy in obtaining the intermediate points was usually much better, because the points where the intermediate trajectories intercepted the cylinder were much better defined than were those of the tangent trajectories (figs. 4 and 5). The tolerances are approximately  $\pm 0.001$  for  $y_0$  and  $\pm 0.012$  radian for  $\theta$ .

Local rate of droplet impingement. - The local rate of water impingement per unit of area on the cylinder surface located at a given angle  $\theta$  can be determined from the relation

$$W_\beta = U_w \frac{dy_0}{d\theta} = U_w \beta \quad (11)$$

provided  $\theta$  is measured in radians. The magnitude of the term  $dy_0/d\theta$  is the fractional part of the maximum water that could impinge on a local area of the cylinder, if all the trajectories were parallel to each other and the cylinder surface were projected into a plane perpendicular to the trajectories. A value of

$$\frac{dy_0}{d\theta} = \beta = 1$$

indicates that the intensity of impingement on a local area of the cylinder is the maximum possible for the liquid-water content present in the cloud. For a uniform cloud composed of droplets all of the same size the value of  $\beta$  is obtained from the slope of the curves of  $y_0$  as a function of  $\theta$  presented in figure 9. Curves of  $\beta$  that correspond to the data of figure 9 are presented in figure 10. The rate of droplet impingement is highest at the stagnation point ( $\theta = 0$ ).

Curves of  $\beta$  as a function of  $\theta$  in addition to those curves given in figure 10 can be found from the relation

$$\beta = \frac{\pi}{2} \frac{E_m}{\theta_m} \cos \left( \frac{\pi}{2} \frac{\theta}{\theta_m} \right)$$



where  $\theta$  is measured in radians. This relation applies on the assumption that the curves in figure 9 are sine curves for which the amplitude is characterized by  $y_{0,m}$  and the period by  $\theta_m$ . The values of  $y_{0,m} = E_m$  and  $\theta_m$  are obtained from figures 6 and 7, respectively.

#### EVALUATION OF ROTATING MULTICYLINDER METHOD

An important application of droplet-trajectory data with respect to cylinders has been in the measurement of droplet size in icing clouds. Several cylinders of different diameters are exposed from an airplane in flight to the supercooled droplets in the icing cloud (fig. 1). It is assumed that all the supercooled droplets that strike the cylinders freeze completely onto the cylinders. The liquid-water content and droplet-size distribution in the cloud are determined by a comparison of the measured weight of ice collected on each of the cylinders with the amount of droplet impingement obtained from the calculated water-droplet trajectories for cylinders of the same size and for the same flight atmospheric conditions. This technique of analyzing icing clouds is described in references 3 and 9 and in appendix D.

Droplet-size distribution patterns. - The data presented in figures 4 through 10 apply directly only to clouds composed of droplets all of which are uniform in size. In a cloud in the earth's atmosphere, the water droplets are often not of uniform size. For a cylinder exposed in a cloud with a given droplet-size distribution pattern, the trajectory data in the figures cited are used to compute other curves that are applicable to the distribution pattern under consideration.

Five different droplet-size distribution patterns have been defined in reference 3 for convenience in the classification of clouds. The table of distribution patterns, reproduced herein as table II, was adopted to cover some of the range encountered in nature. Although the five distributions given in table II are not the only probable patterns existing in clouds, these five distributions are used herein to evaluate the sensitivity and the accuracy that can be expected from the rotating multicylinder method. The method of evaluation applied to these patterns can be used for a similar study of other droplet-size distribution patterns. The droplet-size ratios given in table II are the average radius of the droplets in each group to the radius  $a_0$  of the volume-median droplet size. (The amount of water in all the droplets of a diameter greater than the volume-median droplet diameter is equal to the amount of water in all the droplets of smaller diameter. Volume-median droplet diameter is often referred to as "mean-effective drop diameter." The subscript  $o$  refers to the volume-median condition.) The different distribution patterns have been labeled with the first five letters of the alphabet. A cloud with an A distribution is composed of droplets which are all uniform in size. In a cloud with a

B distribution, 30 percent of the water is contained in the droplets having the volume-median droplet diameter, 20 percent of the water is contained in droplets with a diameter 0.84 as large as the volume-median droplet diameter, and another 20 percent of the water is contained in droplets with a diameter 1.17 times as large as the volume-median droplet diameter. The remaining water is distributed as follows: 10 percent in droplets with a diameter 0.72 as large as the volume-median diameter, 10 percent in droplets 1.32 times as large as the volume-median diameter, 5 percent in droplets 0.56 as large, and 5 percent in droplets 1.49 times as large as the volume-median diameter. A similar interpretation applies to the other distributions listed in table II.

Over-all weighted collection efficiency. - In a cloud composed of droplets of many different sizes, a cylinder of a given diameter will collect some droplets of every size; however, the collection efficiency with the smaller droplets will be less than with the larger droplets. For any assumed droplet-size distribution in the cloud, such as distribution B in table II, an over-all weighted collection efficiency for a cylinder can be calculated from the results of figure 6 by adding together the weighted collection efficiencies that are appropriate to each droplet-size group in the B distribution. For example, 30 percent of the water in all the droplets in the cloud is assumed to be processed by the cylinder at the collection efficiency pertaining to the volume-median droplet; 20 percent of the water in all the droplets in the cloud is assumed to be processed by the cylinder at the lower collection efficiency that applies to droplets with diameters 0.84 as large as the volume-median droplet diameter, and so forth. The over-all weighted collection efficiency for each cylinder in the set of cylinders exposed from the airplane can be calculated for the assumed distribution. A different curve of over-all weighted collection efficiency as a function of cylinder diameter will exist for each assumed droplet-size distribution.

Comparison curves. - The droplet-size distribution prevailing in a cloud at the time of measurement can be found by comparing the shape of a curve of cylinder diameter as a function of the measured ice accumulated per unit area in flight on each cylinder (fig. 11) with the shape of the calculated curves of cylinder diameter as a function of over-all weighted collection efficiency. Sets of calculated curves for comparison are shown in figure 12 for the droplet-size distributions A through E of table II. The detailed method of calculation of these curves, which differs slightly from that presented in reference 3, is discussed in appendix D. The ordinate in figure 12 is the reciprocal of the inertia parameter  $(1/K)_0$  as applied to the volume-median droplet size, and the abscissa is the over-all weighted collection efficiency  $E_w$ . The amount of ice accumulated per unit of cylinder area is directly proportional to the over-all weighted collection efficiency. The comparison is valid provided that the actual droplet-size distribution prevailing in the cloud during the cylinder exposure was one of the assumed distributions for which comparison curves are available.

The term  $(1/K)_o$ , rather than the diameter of the cylinders in a set of cylinders, is used for the ordinate, because  $(1/K)_o$  is directly proportional to the cylinder diameter through the relation

$$(1/K)_o \equiv \frac{9}{2} \frac{\mu L}{\rho_w a_o^2 U} \quad (12)$$

The direct proportionality between  $(1/K)_o$  and  $L$  applies to the data obtained during one run, because all the different sized cylinders in the set of cylinders are exposed to the same air viscosity, free-stream velocity, water density, and volume-median droplet diameters in the cloud. The use of  $(1/K)_o$  as ordinate permits the use of the curves in figure 12 for a large number of combinations of different flight conditions.

In the preceding explanation of a method for obtaining the droplet-size distribution in the cloud, it was tacitly assumed that another method was also available for obtaining the volume-median droplet size. A method has been devised which takes into consideration the volume-median droplet size by combining the parameter  $\varphi$  and the inertia parameter  $K$  into another parameter

$$(K\varphi)_o \equiv \left( \frac{2\rho_a a_o U}{\mu} \right)^2 \equiv (Re_o)_o^2 \quad (13)$$

The only unknown quantity in this parameter is the volume-median droplet size  $a_o$ . In order to cover the more probable conditions of airplane speed, air viscosity and density, and volume-median droplet size, values of  $(K\varphi)_o$  ranging from 0 to 10,000 were chosen for the calculations and are presented in figure 12. After the flight data involving cylinder size and ice collected (fig. 11) are matched to one of the curves in figure 12, the value of  $(1/K)_o$  in figure 12 corresponding to a cylinder with radius  $L$  of unity is noted when figures 12 and 11 are superimposed. The volume-median droplet size is computed from equation (12) for the particular  $(1/K)_o$  obtained from figure 12 and the known flight conditions. A more detailed procedure for obtaining the droplet-size distribution and the volume-median droplet size is discussed in appendix D.

The liquid-water content is obtained by extrapolating the icing rate measured by the set of cylinders to an infinitely small cylinder with unity collection efficiency. This procedure, as described in appendix D, determines the ice collected by a cylinder that collects all the water in its path.

Matching flight data. - A manner for plotting flight results involving the cylinder diameter as a function of the ice accumulated on each cylinder in grams per second per square inch of frontal area is illustrated in figure 11. The data plotted in figure 11 for the four cylinders used in flight (diameters of 3,  $1\frac{1}{4}$ ,  $\frac{1}{2}$ , and  $\frac{1}{8}$  in.) are shown in figure 13 matched to some of the curves taken from figure 12. The method used for matching the data is described in appendix D. In order to simplify the illustration, only portions of the best fitting curves of figure 12 are shown superimposed on the data in figure 13. The ordinates of figure 12 are not shown, except that the value of  $(1/K)_0$  where  $L = 1$  is given on each of the curves taken from figure 12.

A practical difficulty arises in matching the flight data with the curves of figure 12. The difficulty is caused by the scattering of the measured data due to errors in the measurements, by the difference between the assumed theoretical distributions on which the curves of figure 12 are based and the conditions actually prevailing in the natural cloud during the time the cylinders were exposed, and by the inherent extreme insensitivity of the rotating multicylinder method to differences in droplet-size distributions even if the preceding difficulties were not present. The possible errors in measurement include those caused by errors in measuring flight speed, exposure time, and air temperature, differences between the exposure time of the large cylinder and the small cylinder due to the time required to extend and retract the set, losses in the accumulated ice while disassembling the cylinders prior to weighing, failure of droplets to freeze on the cylinders, and errors in weighing. Another error that determines the accuracy of the final answer is the expected error in the calculation of over-all weighted collection efficiency plotted in figure 12. This error has been determined to be as large as 2 percent (appendix D). Experience in obtaining flight data has shown that the accrued error from all sources can be maintained below  $\pm 10$  percent but seldom can be expected to be less than  $\pm 5$  percent.

The hypothetical data points of figure 11 were chosen to fit precisely the curve for the B distribution given in figure 12(e) (volume-median droplet diameter for the data of fig. 11 was assumed to be 20 microns). If the data were flight data taken in a cloud in which the droplet sizes were defined by a B distribution and the volume-median droplet size were 20 microns, the data would probably not fit the B distribution of figure 12(e) precisely, but each point would deviate by an amount which depended on the accrued error related to the care in measuring. The braces in figure 11 indicate the range of a  $\pm 5$ -percent error, and the brackets indicate the range of a  $\pm 10$ -percent error. In the analysis of the flight data, the magnitude of the accrued error will affect the answers obtained and will determine the sensitivity of the multicylinder method.

Expected errors in analysis of flight data. - An attempt is made herein to evaluate the sensitivity of the multicylinder method when errors of known magnitude are present in the flight data. The expected error in the calculation of over-all weighted collection efficiency plotted in figure 12 could be shown graphically in terms of the width of the lines used to plot the curves of figure 12. When the calculated curves of figure 12 are superposed on the flight data of figure 11 for comparison, the error in calculating over-all collection efficiency can be added to the error in measuring and both errors included in the range indicated by the braces (or brackets) and termed an accrued error.

Three sections of different curves taken from figure 12(e) are shown in figure 13 to come within the  $\pm 5$ -percent range of accrued errors. The following is an illustrative example in the interpretation of the material presented in figure 13: If measurements were made simultaneously by a large number of careful observers who kept the accrued error within  $\pm 5$  percent at a true airspeed of 200 miles per hour in a cloud in which the volume-median droplet size was actually 20 microns in diameter and the droplet-size distribution was defined by the B distribution of table II, the final answers reported by the observers would vary from 17 to 25 microns for the diameter of the volume-median droplet and from an A distribution to an E distribution.

The type of analysis described with the use of figure 13 was made to cover a range of true flight speed up to 400 miles per hour and to cover actual volume-median droplet sizes up to 30 microns in diameter.

A set of four cylinders with diameters of 3,  $1\frac{1}{4}$ ,  $\frac{1}{2}$ , and  $\frac{1}{8}$  inches was assumed for the analysis. The other secondary variables assumed were an altitude of 10,000 feet and air viscosity of  $3.436 \times 10^{-7}$  slugs per foot-second. The errors that can be expected in the final answers of the volume-median droplet size for accrued errors of  $\pm 5$  and  $\pm 10$  percent (including the expected error in the calculations for the theoretical data of fig. (12)) are shown in figures 14(a) and 14(b), respectively. The ordinate is the error possible in reporting the actual volume-median droplet size in a cloud. An upper and lower limit are shown in the figures. Usually, it is possible to have a larger magnitude of error in reporting the size too large than the magnitude of error in reporting the size too small. For example, in a cloud in which the droplet size was actually 30 microns in diameter and the true airspeed was 200 miles per hour (accrued error =  $\pm 5$  percent, fig. 14(a)), the answer reported would be within the limits of 25 and 40 microns. The lower limit error is approximately 18 percent, and the upper limit error is approximately 35 percent.

Doubling the sizes of the cylinders has the same effect on error as halving the flight speed. If a set of cylinders of 6-,  $2\frac{1}{2}$ -, 1-, and

$\frac{1}{2}$ -inch diameter were used at a flight speed of 200 miles per hour, the expected error can be found from the curves of figure 14 for a flight speed of 100 miles per hour. The expected error in the final results increases rapidly with increasing droplet sizes and flight speeds. The value of the multicylinder method in clouds consisting of volume-median droplet sizes above 30 microns in diameter is questionable, if the airplane speed cannot be maintained below 100 miles per hour.

The accuracy in the determination of the droplet-size distribution is very much subject to personal discrimination as well as to errors in measurements. The same measured data resolved by different observers often result in large differences in the typing of the distributions. If  $\pm 5$ -percent accrued error in measurements is assumed, the insensitivity of the multicylinder method does not permit an A distribution to be distinguished from an E distribution with data taken at flight speeds above 150 miles per hour.

Careful determinations of liquid-water content are usually not in error by more than  $\pm 5$  percent, provided the size of the smallest cylinder is  $\frac{1}{8}$  inch in diameter or less and the measuring errors are less than  $\pm 4$  percent. The error in determining liquid-water content is usually 1 percent larger than the total errors in the measurements, because the curves of figure 12 are accurate only within  $\pm 1$  percent at low values of  $(1/K)_0$ .

Lewis Flight Propulsion Laboratory  
National Advisory Committee for Aeronautics  
Cleveland, Ohio, September 5, 1952

## APPENDIX A

## SAMPLE MACHINE SETUP FOR CALCULATING WATER-DROPLET TRAJECTORIES

Principle of operation. - The water-droplet trajectories were computed on a mechanical analog which was fundamentally a differential analyzer constructed for solving the equations of motion (equations (1) and (2)). Although the operational theory and technique of preparing a problem for solution on a mechanical differential analyzer have been reported (references 12 to 14), the principles of operation of the mechanical analogy are reviewed herein, and a machine setup together with all the pertinent computations involved for a representative trajectory are presented.

The mechanical analog, shown in figure 15, consists of a number of computing units interconnected by a system of shafts and gears. Each unit performs mechanically one of the operations involved in the solution of the differential equations, such as integration and algebraic addition. The computational process of the analog is purely kinematic and not dynamic; any interruption in the solution or change of rate of solution by the operator does not affect the final result. The machine can evaluate only particular numerical solutions of particular equations in which all coefficients have numerical values and for which numerical initial conditions are known. A formal solution cannot be obtained from the machine.

The principal unit of a differential analyzer is the integrator, six of which are on the analog shown in figure 15. When an expression is integrated on a differential analyzer, the integrating unit provides a continuously variable rate of change of the variables and derivatives, thereby preserving the essential feature of the calculus. Thus, if the magnitude of the independent variable  $\tau$  were measured by the number of revolutions of a driving shaft arranged to drive a second shaft through a coupling gear ratio  $N$ , a rotation  $d\tau$  of the driving shaft will result in a rotation  $Nd\tau$  of the driven shaft. If the coupling ratio changes while the driving shaft is rotating, the total rotation  $y$  of the driven shaft is

$$y = \int Nd\tau$$

A continuously variable coupling ratio that can pass through zero and provide for positive and negative signs is achieved with a modified Kelvin disk integrator, shown in figure 16. The rotation of the horizontal disk, the axis of which is fixed, is transferred to the roller through a pair of balls. The coupling ratio between the disk and the roller may be changed by varying the position of the balls across the diameter of the disk. If the point of contact between the balls and

the disk is a distance  $\eta$  from the center of the disk and if the disk rotates an amount  $d\tau$ , the roller will rotate through  $\frac{\eta}{\lambda} d\tau$  turns, where  $\lambda$  is the radius of the roller. In the integrators used on the analog, the distance  $\eta$  is varied by means of a lead screw that displaces the ball carriage across the diameter of the disk.

For convenience, all quantities are expressed in terms of shaft rotations. The expression for the rotation of the roller previously derived as  $\frac{1}{\lambda} \int \eta d\tau$  is rewritten in terms of the rotation of the shaft that drives the disk, the lead screw shaft that displaces the ball carriage, and the integrator roller. The number of turns  $\xi$  of the integrand shaft required to produce a linear displacement  $\eta$  of the ball carriage is equal to  $\eta/p$ , where  $p$  is the effective pitch of the lead screw. The radius of the roller, the pitch of the lead screw, and other gear ratios permanently installed in the integrator to facilitate the driving of the lead screw are collected together in a term referred to as the integrator constant  $\Gamma$ . The expression for the rotation of the roller becomes  $\Gamma \int \xi d\tau$ .

Large torques cannot be transmitted through the integrator without slippage between disk, balls, and roller. Very low torques are imposed on the integrators. The torque required to drive the gear trains, shafts, and other computing elements in the mechanical circuit beyond the integrator is obtained from a torque amplifier placed in the circuit immediately after the integrator.

Algebraic additions are performed by mechanical gear differentials, which operate in principle similarly to the differentials used to drive the rear wheels on conventional automobiles. The purpose of the differentials used in the analog is to combine two rotating inputs into one rotating output, which for the analog differentials is one-half the algebraic sum of the inputs. A high-precision spur-gear differential with practically instantaneous response is used in the analog.

Sample computation of gearing required. - The problem of constraining the basic computing elements (integrators, differentials, and input intelligence) to solve the differential equations (equations (1) and (2)) is approached in three steps. The first step is the preparation of a pictorial diagram showing how the various computing units are interconnected, without regard to scale factor. A pictorial diagram for the solution of equation (1) is shown in figure 17. A similar diagram is used to solve equation (2). In order to adapt the equations of motion to a convenient form for the analog, equation (1) is rewritten as



$$\frac{dx}{d\tau} = \frac{1}{K} \int v \sigma_x d\tau \quad (A1)$$

where

$$v \equiv \frac{C_D Re}{24} \quad \text{and} \quad \sigma_x \equiv \left( u_x - \frac{dx}{d\tau} \right)$$

The second step is the introduction of appropriate gear ratios into the pictorial diagram to provide proper scale factors between each computing element. These gear ratios are introduced as ratios  $n_1, n_2, \dots, n_n$  to each integrand shaft of the integrators and to the inputs and outputs of each differential. The purpose of the gear ratios is to ensure that the ranges of the derivative functions introduced as integrand quantities to the integrators do not exceed the mechanical translation limits of the ball carriage and to provide equal scale factors for quantities being added in a single differential adding unit. A schematic diagram that aids in evaluating the gear ratios is shown in figure 18.

The constant coefficients preceding each variable quantity in figure 18 represent the number of revolutions a particular shaft must make to represent one unit of that particular quantity. For example, shaft number 1 has a coefficient  $An_1$  and the variable is  $u_x$ , which may be interpreted as  $An_1$  revolutions of shaft number 1 representing one unit of  $u_x$ .

The coefficients A, B, and C are scale factors for the sources of intelligence fed to the machine. The input chart, from which the intelligence required by the machine for the local air velocity  $u_x$  is fed to the machine by an operator, was drawn to a size such that 96 revolutions of the input-chart lead screw represent one unit of  $u_x$ ; therefore,  $A = 96$ . The coefficient B was chosen to equal 128 revolutions of the independent-variable drive motor to represent one unit of time. The coefficient C was chosen to equal 8 because of convenience in using available gearing. The resultant quantities, shown in the two columns at the extreme right of figure 18, are evaluated from the equations of constraint to be presented.

In order that the variables  $u_x$  and  $dx/d\tau$  be added algebraically in the differential, the number of revolutions of the  $u_x$  input shaft (shaft 1, fig. 18) per unit of  $u_x$  must equal the number of revolutions of the  $dx/d\tau$  shaft (shaft 2) per unit of  $dx/d\tau$  at the input to the differential. This equality suggests a need for the gear ratio  $n_4$  between shafts 2 and 8.

Equation (A1) may be written in terms of the constant coefficients shown in figure 18 such that

$$\frac{An_1}{n_4} \frac{dx}{d\tau} = \frac{ABC}{512} n_1 n_2 n_3 n_6 \int v \sigma_x d\tau$$

$$\frac{dx}{d\tau} = \frac{BC}{512} n_2 n_3 n_4 n_6 \int v \sigma_x d\tau \quad (A2)$$

This expression is obtained from figure 18 by equating the motion of shaft 8 with the motion of shaft 7 after the motion of shaft 7 has passed through the gear ratio  $n_6$ . From a comparison of equation (A2) with equation (A1)

$$\frac{1}{K} \equiv \frac{BC}{512} n_2 n_3 n_4 n_6 \quad (A3)$$

In order to assure that the integrand of integrator I (fig. 18) does not exceed the limit of translation of the ball carriage;

$$\frac{An_1 n_2}{2} \sigma_{x,m} \leq 192 \quad (A4)$$

because the integrand lead screw can make 192 revolutions within the mechanical limits. Two other equations of constraint can be obtained by applying the same constraint to the integrand of integrators II and III, respectively:

$$Cn_3 v_m \leq 48 \quad (A5)$$

and

$$\frac{An_1 n_5}{n_4} \left( \frac{dx}{d\tau} \right)_m \leq 192 \quad (A6)$$

The input chart from which the  $u_x$  intelligence is fed to the machine is wrapped around one of the two input drums, as shown in figure 15. The x-coordinate of this chart is laid off around the circumference of the drum. The x-displacement of the droplet from the starting point (5 radii ahead of the center of the cylinder) must not exceed one revolution of the drum. The equation that defines this constraint is

$$\frac{AB}{32} \frac{n_1 n_5 n_7}{n_4} x_{\text{range}} \leq 1 \quad (A7)$$

The maximum and minimum values of all the variables appearing in equations (A3) to (A7) must be known or intelligently estimated. For the example presented herein, the following excursions of the variables were assumed:

$$\left. \begin{aligned}
 0 &\leq x \leq 5 \\
 0 &\leq u_x \leq 2 \\
 0 &\leq \frac{dx}{dt} \leq 2 \\
 0 &\leq \sigma_x \leq 1 \\
 1 &\leq v \leq 6 \\
 \frac{1}{2} &\leq K \leq 4
 \end{aligned} \right\} \quad (A8)$$

The results presented in figure 9 cover a range of values of  $K$  from 0.25 to 320. Several machine setups were required to solve that large range of variation in  $K$ . For this example, the range of  $K$  is limited from  $1/2$  to 4. The changes in  $K$  are made by changing the gear ratio  $n_6$ . In order to cover the range of values of  $K$  assigned to this machine setup without requiring inconveniently large gear ratios for  $n_6$ , a value of  $K = 1$  is assigned to equation (A3) when  $n_6 = 1$ . With these values of  $K$  and  $n_6$ , equation (A3) reduces to

$$n_2 n_3 n_4 BC = 512 \quad (A9)$$

The gear ratio  $n_7$  can be obtained from the simultaneous solution of equations (A6) and (A7). The ratio chosen was  $n_7 = \frac{1}{2250} = \left(\frac{1}{900}\right)\left(\frac{3}{5}\right)\left(\frac{2}{3}\right)$ , because this ratio was easily formed with the available change gears. The input and output chart scales were such that five units of  $x$  were equal to  $\frac{1920}{2250}$  revolutions of the drums. The ratio  $n_3 = 1$  is obtained from equation (A5). The relation

$$n_1 n_2 n_5 \leq \frac{1}{2} \quad (A10)$$

is obtained from expressions (A6) and (A9). From this relation and equation (A4),

$$n_5 = \frac{1}{8}$$

which required (from expression (A10)) that  $n_1 n_2 = 4$ . The gear ratios  $n_1 = 4$  and  $n_2 = 1$  are taken as such by choice because of ease in applying these ratios in the machine. From equation (A9),  $n_4 = \frac{1}{2}$ .

A similar computational procedure is done for equation (2). The gear trains for the solutions of equation (1) and (2) are combined in a plan view, as shown in figure 19, in which the computed gear ratios are shown in position. The plan view of figure 19, which is the third step, is very similar to the actual machine setup (fig. 15) and is used to assemble the final setup.

The values of  $u_x$  and  $u_y$  are fed to the machine continuously by the operators from the two end input drums shown in figure 15. The droplet trajectories (fig. 4) are plotted by the machine on the center drum on a sheet of acetate in order to minimize errors caused by changes in humidity and temperature during the calculations. The y-ordinate is scaled to four times the x-ordinate in order to gain accuracy in reading the  $y$  and  $\theta$  values. The values of  $C_D Re/24$  are varied continuously during the computation of the trajectories and are determined with the use of equation (5) and tables in references 3 or 6. The values of  $(u_x - v_x)$  and  $(u_y - v_y)$  are obtained from counters on the machine during the calculations.

## APPENDIX B

STARTING CONDITIONS OF TRAJECTORIES AT LARGE VALUES OF  $-x$ 

For practical reasons the integration of the differential equations of motion (equations (1) and (2)) cannot be started with the NACA analog from an infinite distance ahead of the cylinder. The equations are therefore linearized by an approximation up to a convenient distance ahead of the cylinder. The method of linearizing the equations is presented in reference 3 and results in the following expressions:

$$v_x = 1 - \frac{M(\beta)}{x^2}$$

$$v_y = \frac{1 - M(\beta)y_0}{Kx^2} - \left(\frac{2y_0}{x^5}\right) (1 - 2y_0)^2$$

$$\Delta y = \frac{M(\beta)y_0}{x^2} + \frac{(1-y_0)^2 y_0}{x^4}$$

$$M(\beta) = \beta + \beta^2 e^\beta E_1(-\beta)$$

$$\beta = -\frac{x}{K}$$

The symbols for these expressions are the same as those used in reference 3. The exponential integral  $E_1(-\beta)$  is tabulated in pages 1 through 9 of reference 15. The y-ordinate of the droplet is found by adding  $\Delta y$  to  $y_0$ .

For the studies of the trajectories discussed herein, the integration of equations (1) and (2) with the NACA analog was always started at  $x = -5$ . The accuracy of the preceding linearized starting equations was checked by integrating equations (1) and (2) for  $K = 32, 16,$  and  $4$  with the NACA analog from  $x = -50$  to  $x = -5$ . The difference in results was within the expected accuracy of the analog. The preceding linearized starting equations were found to be invalid for values of  $K$  less than  $0.5$ . For values of  $K$  less than  $0.5$ , the equations gave values of  $v_y$  greater than the corresponding values of  $u_y$  and values of  $v_x$  smaller than the corresponding values of  $u_x$ . For values of  $K$  less than  $0.5$ , the starting conditions at  $x = -5$  were assumed to be the same as those conditions prevailing for the air streamlines. This assumption is valid, because the droplet inertias are very small.

## APPENDIX C

## CONVERSION OF PRACTICAL FLIGHT UNITS INTO DIMENSIONLESS

PARAMETERS  $K$ ,  $\varphi$ , AND  $Re_0$ 

The following relations are presented to aid in the interpretation of free-stream velocity (airplane speed), cylinder diameter, air viscosity, air and water density, and droplet diameter in terms of the dimensionless parameters  $K$ ,  $\varphi$ , and  $Re_0$  used in this report:

$$K = 4.088 \times 10^{-11} \left( \frac{d^2 U}{\mu D} \right) \quad (C1)$$

$$Re_0 = 4.813 \times 10^{-6} \left( \frac{d \rho_a U}{\mu} \right) \quad (C2)$$

$$d = 1.564 \times 10^5 \sqrt{\frac{K \mu D}{U}} \quad (C3)$$

$$\varphi = 0.567 \frac{\rho_a^2 D U}{\mu} \quad (C4)$$

$$K \varphi = 2.316 \times 10^{-11} \left( \frac{d \rho_a U}{\mu} \right)^2 \quad (C5)$$

$$\rho_a = 0.0412 \frac{p}{T_a} \quad (C6)$$

$$W_m = 2.745 \times 10^{-2} E_m D U w \quad (C7)$$

$$W_\beta = 0.3294 U w \beta \quad (C8)$$

$$w = 3466 \frac{M_m}{U} \quad (C9)$$

where

$D$  cylinder diameter, in.

$d$  droplet diameter, microns

$E_m$  collection efficiency (fig. 6), dimensionless

$K$  inertia parameter, dimensionless

$M_m$	ice accumulation for cylinder with $E_w = 1.0$ , g/(sq in.)(sec)
$p$	absolute atmospheric pressure, in. Hg
$Re_0$	free-stream Reynolds number with respect to droplet
$T_a$	air temperature, °R
$U$	true flight speed, mph
$W_m$	rate of water interception, lb/(hr)(ft span)
$W_\beta$	local rate of water interception, lb/(hr)(sq ft)
$w$	liquid-water content, g/cu m
$\beta$	local impingement efficiency, dimensionless
$\mu$	air viscosity, slugs/(ft)(sec)
$\rho_a$	air density, slugs/cu ft
$\phi$	altitude parameter, dimensionless

(The density of water was assumed to be 62.46 lb/cu ft; and the acceleration due to gravity, 32.17 ft/sec<sup>2</sup>.)

## APPENDIX D

METHOD OF CALCULATING CURVES OF  $(1/K)_0$  AGAINST  $E_{\omega}$  FOR DIFFERENT  
 ASSUMED DROPLET-SIZE DISTRIBUTIONS AND USE OF CURVES  
 IN ROTATING MULTICYLINDER METHOD

In the rotating multicylinder method of measuring droplet-size distributions and liquid-water content in a cloud, several cylinders of different diameters are exposed simultaneously from an airplane in flight to the supercooled droplets in the cloud. During the exposure time all the cylinders are subjected to the same conditions of flight speed  $U$ , air viscosity  $\mu$ , air density  $\rho_a$ , water density  $\rho_w$ , and cloud droplet sizes and number approaching the cylinders from the undisturbed cloud. The variable among the cylinders is the cylinder size  $L$  and, consequently, the collection efficiency of each cylinder. An increase in  $L$  will decrease  $K$  (equation (3)) for any given droplet size  $a$  and thereby decrease the collection efficiency of the cylinder for that particular droplet size (fig. 6). Each successively larger cylinder in the exposed set of cylinders will collect a smaller percentage of the droplets of any one given size. The  $K\Phi$  parameter defined by equation (13) is constant, because it does not contain  $L$ .

In a cloud composed of droplets of many different sizes, a cylinder of a given diameter will collect some droplets of every size; however, the collection efficiency for the smaller droplets will be less than for the larger droplets. For any assumed droplet-size distribution in the cloud, such as distribution B in table II, an over-all collection efficiency for a cylinder can be calculated from the results of figure 6 by adding together the weighted collection efficiencies that are appropriate to each droplet-size group in the B distribution.

The procedure for obtaining the over-all weighted collection efficiency (fig. 12) is explained with the use of a sample calculation for the B distribution of table II and an assumed  $(K\Phi)_0$  of 200 (equation (13)). The over-all weighted collection efficiency of one cylinder in a group of cylinders is given as the final result in table III. As a basis for beginning the computation, a value of  $1/K = 4.0$  is assigned to those droplets in the volume-median group size. (This particular value of  $1/K$  is chosen arbitrarily and will define one point on the curves of  $(1/K)_0$  against  $E_{\omega}$  for  $(K\Phi)_0 = 200$  of figure 12(b). A value of the collection efficiency for  $K = 1/4.0$  is found in figure 6 and is given in the fifth column of table III. The required value of  $\Phi$  is obtained from the original assumption that  $(K\Phi)_0 = 200$ ; therefore,  $\Phi = 800$  for  $(1/K)_0 = 4.0$ . The weighted



collection efficiency is found by taking the product of the percentage water in each size group (column 3) and the collection efficiency of column 5. The weighted collection efficiency is recorded in column 6. The effect of the variation of the group size on  $1/K$  is obtained by dividing the value of  $1/K$  assigned to the volume-median droplet size ( $1/K = 4.0$  in this example) by  $(a/a_o)^2$ , because the droplet radius appears to the second power in equation (3). The change in  $K$  with the change in droplet size is recorded in column 4. A value for the collection efficiency is found from figure 6 for each value of  $K$  in column 4. The value of  $\varphi$  remains the same as for the volume-median droplet size ( $\varphi = 800$ ) because the droplet size does not enter into the definition of  $\varphi$  (equation (7)).

The weighted collection efficiency is again the product of the values in column 3 and the collection efficiency of column 5. The sum of the individual weighted collection efficiencies of column 6 is the over-all weighted collection efficiency. The sum at the bottom of column 6 in table III(a), in combination with the assigned value of  $(1/K)_o$  to the volume-median droplet size, defines one point on the B-distribution curve of figure 12(b).

In order to obtain another point for the B-distribution curve of figure 12(b), a different value is assigned to  $1/K$  for the volume-median droplet size; for example, in table III(b)  $(1/K)_o = 1.0$  as compared with  $(1/K)_o = 4.0$  in table III(a). The lowering of the value of  $(1/K)_o$  has the same effect as decreasing the cylinder size  $L$  when the physical dimensions of the volume-median droplet size, air-plane speed, water density, and air viscosity are maintained constant (equation (3)), as is actually the physical condition when a set of different-sized cylinders are flown simultaneously through a cloud. The procedure for computing the values in columns 4, 5, and 6 is the same as was described for table III(a). The only exception is that the value of  $\varphi$  is now changed to 200 in order to maintain  $(K\varphi)_o = 200$  for  $(1/K)_o = 1.0$ . The value of  $\varphi$  is maintained at 200 during the calculations for table III(b).

The calculations of reference 3 apparently are different from those described herein, in that in the calculations of reference 3,  $\varphi$  appears to have been allowed to vary to conform with maintaining  $K\varphi$  constant during the calculations for the weighted collection efficiency. The value of  $\varphi$  cannot be permitted to vary during the calculations of the over-all weighted collection efficiency, because airplane speed, cylinder size, air density, air viscosity, and water density are not variables during that phase of the calculations.

The over-all weighted collection efficiencies, which are the sums at the bottom of column 6 in table III, are tabulated in table IV for

the values required to draw the curves of figure 12. The values of table IV are subject to a tolerance error caused by the limit of accuracy in obtaining the collection efficiencies from the trajectories computed with the analog. The expected error in determining the collection efficiency for droplets with low inertia was much greater than for those with large inertia. The expected root mean square error of the over-all weighted collection efficiencies of table IV, based on the expectation of individual random errors, was determined from the following expression:

$$\Delta H = \sqrt{(0.05)^2(\Delta a)^2 + (0.10)^2(\Delta b)^2 + (0.20)^2(\Delta c)^2 + (0.30)^2(\Delta d)^2 + (0.20)^2(\Delta e)^2 + (0.10)^2(\Delta f)^2 + (0.05)^2(\Delta g)^2}$$

where  $\Delta a$ ,  $\Delta b$ , and so forth are actual errors in determining the respective collection efficiency. The expected root mean square error in the curves of figure 12 has been determined to be somewhat less than 1 percent for values of  $E_{\omega}$  near 1.0 and approximately 2 percent for values of  $E_{\omega}$  near 0.01.

The droplet-size distribution and volume-median droplet size in a cloud are determined by comparing the measured values obtained from a set of rotating multicylinders with curves of figure 12. On log-log paper of the same scale factor as that in figure 12, the measured weight of ice accumulated per unit of projected cylinder area is plotted as the abscissa and the cylinder diameter is plotted as the ordinate (fig. 11). The curve of figure 12 that best fits the data of figure 11 is found by superimposing the data of figure 11 on the curves of figure 12 and shifting the two sheets, one with respect to the other, horizontally and vertically (not rotated). The horizontal and vertical shifting is permitted, provided the plots are on log-log paper, because  $E_{\omega}$  and the amount of ice per unit projected cylinder area are proportional and because  $(1/K)_0$  is proportional to the cylinder diameter  $2L$ . The matching of the curves must also fulfil the condition that equations (3) and (13) must be satisfied simultaneously. The value of  $(1/K)_0$  in figure 12 corresponding to a cylinder with radius  $L$  of unity is noted while figures 12 and 11 are superimposed. For these values of  $(1/K)_0$  and  $L$ , a value of  $a_0$  can be found from equation (3), because  $\rho_w$ ,  $\mu$ , and  $U$  are known flight measurements. The calculated value of  $a_0$  is used to determine the value of  $(K\Phi)_0$  from equation (13). If the value of  $(K\Phi)_0$  determined by this method does not correspond with the  $(K\Phi)_0$  sheet of figure 12 used for the matching, a different match must be found on a different  $(K\Phi)_0$  curve sheet. A method for approximating and interpolating is described in reference 9.

After the curve that best fits the data has been found, the droplet-size distribution of the cloud is found by noting the letter on the curve in figure 12. The volume-median droplet size is that value which satisfies equations (3) and (13) simultaneously. The liquid-water content of the cloud is determined by noting the value of ice accumulation where the ordinate  $E_w = 1.0$  crosses the abscissa of figure 11 while figures 12 and 11 are superimposed. This procedure has the effect of extrapolating the icing rate measured by the set of cylinders to an infinitely small cylinder with unity collection efficiency. The value of ice accumulation  $M_m$  of the abscissa where  $E_w = 1.0$  is substituted in the following relation:

$$w = 3466 \frac{M_m}{U}$$

where  $M_m$  is in grams per square inch per second and  $U$  is in miles per hour in order to obtain  $w$  in grams per cubic meter.

#### REFERENCES

1. Glauert, Muriel: A Method of Constructing the Paths of Raindrops of Different Diameters Moving in the Neighborhood of (1) a Circular Cylinder, (2) an Aerofoil, Placed in a Uniform Stream of Air; and a Determination of the Rate of Deposit of the Drops on the Surface and the Percentage of Drops Caught. R. & M. No. 2025, British A.R.C., 1940.
2. Ranz, W. E.: The Impaction of Aerosol Particles on Cylindrical and Spherical Collectors. Tech. Rep. No. 3, Eng. Exp. Station, Univ. Ill., March 31, 1951. (Contract No. AT(30-3)-28, U.S. Atomic Energy Commission.)
3. Langmuir, Irving, and Blodgett, Katherine B.: A Mathematical Investigation of Water Droplet Trajectories. Tech. Rep. No. 5418, Air Material Command, AAF, Feb. 19, 1946. (Contract No. W-33-038-ac-9151 with General Electric Co.)
4. Brun, Rinaldo J., Serafini, John S., and Gallagher, Helen M.: Impingement of Cloud Droplets on Aerodynamic Bodies as Affected by Compressibility of Air Flow Around the Body. NACA TN 2903, 1953.
5. Kantrowitz, Arthur: Aerodynamic Heating and the Deflection of Drops by an Obstacle in an Air Stream in Relation to Aircraft Icing. NACA TN 779, 1940.

6. Bergrun, Norman R.: A Method for Numerically Calculating the Area and Distribution of Water Impingement on the Leading Edge of an Airfoil in a Cloud. NACA TN 1397, 1947.
7. Bergrun, Norman R.: An Empirical Method Permitting Rapid Determination of the Area, Rate, and Distribution of Water-Drop Impingement on an Airfoil of Arbitrary Section at Subsonic Speeds. NACA TN 2476, 1951.
8. Brun, Rinaldo J., Serafini, John S., and Moshos, George J.: Impingement of Water Droplets on an NACA 65<sub>1</sub>-212 Airfoil at an Angle of Attack of 4°. NACA RM E52B12, 1952.
9. Anon: The Multicylinder Method. The Mount Washington Monthly Res. Bull., vol. II, no. 6, June 1946.
10. Wien, W., and Harms, F. eds.: Handbuch der Experimentalphysik Teil 4, Bd. 4, Akademische Verlagsgesellschaft M.B.H., (Leipzig), 1932.
11. Glauert, H.: The Elements of Aerofoil and Airscrew Theory. The Macmillan Co. (New York), 1944.
12. Bush, V.: The Differential Analyzer. A New Machine for Solving Differential Equations. Jour. Franklin Inst., vol. 212, no. 4, Oct. 1931, pp. 447-488.
13. Kuehni, H. P., and Peterson, H. A.: A New Differential Analyzer. A.I.E.E. Trans., vol. 63, May 1944, pp. 221-227.
14. Crank, J.: The Differential Analyser. Longmans, Green & Co., 1947.
15. Jahnke, Eugen, and Emde, Fritz: Tables of Functions. Dover Pub., 4th ed., 1945.

TABLE I - COMPARISON WITH RESULTS OF REFERENCE 3



$\varphi$	K	$Re_0$	$E_m$		$\theta_m$		$v_x$		$v_y$	
			NACA	Lang-muir	NACA	Lang-muir	NACA	Lang-muir	NACA	Lang-muir
0	0.25	0	0.051	0.042	0.330	-----	0.151	-----	0.438	-----
	.50	---0----	.205	.186	.716	0.688	.573	0.523	.658	0.635
	1	---0----	.380	.380	.980	.991	.817	.827	.547	.542
	4	---0----	.741	.722	1.379	1.365	1.039	1.008	.198	.211
	16	---0----	.920	.909	1.518	1.517	1.018	1.002	.054	.055
	40	---0----	.957	.962	1.538	1.546	1.014	-----	.036	-----
	320	---0----	.995	.997	1.557	1.567	1.005	-----	.016	-----
100	0.50	7.071	0.157	0.127	0.601	0.565	0.445	-----	0.650	-----
	1	10	.309	.296	.865	.857	.717	.915	.612	.793
	4	20	.680	.639	1.291	1.253	1.022	.993	.295	.326
	40	63.246	.924	.928	1.522	1.504	1.018	-----	.050	-----
1,000	0.50	22.361	0.116	0.090	0.504	0.483	0.329	-----	0.596	-----
	1	31.623	.250	.228	.760	.719	.617	-----	.650	-----
	4	63.246	.616	.568	1.20	1.147	.980	-----	.382	-----
	16	126.49	.830	.806	1.445	1.391	1.036	-----	.133	-----
10,000	0.50	70.711	0.070	0.053	0.385	0.384	0.195	-----	0.482	-----
	1	100	.157	.156	.595	.597	.441	0.494	.650	0.725
	4	200	.480	.441	1.060	.997	.890	.877	.500	.567
	16	400	.755	.710	1.345	1.286	1.035	1.039	.239	.304
50,000	0.5	158.114	0.038	0.035	0.267	0.314	0.085	-----	0.310	-----
	1	223.607	.105	.097	.45	.494	.266	-----	.549	-----
	4	447.214	.378	.340	.916	.873	.762	-----	.584	-----
	16	894.427	.682	.615	1.258	1.169	1.009	-----	.327	-----
	320	4000	.940	.912	1.515	1.470	1.020	-----	.058	-----

TABLE II - FIVE ASSUMED DISTRIBUTIONS OF DROPLET SIZE

(REFERENCE 3)



Total liquid water in each size group (percent)	a/a <sub>0</sub>				
	Distributions				
	A	B	C	D	E
5	1.00	0.56	0.42	0.31	0.23
10	1.00	.72	.61	.52	.44
20	1.00	.84	.77	.71	.65
30	1.00	1.00	1.00	1.00	1.00
20	1.00	1.17	1.26	1.37	1.48
10	1.00	1.32	1.51	1.74	2.00
5	1.00	1.49	1.81	2.22	2.71

The size is expressed as the ratio of the average drop radius in each group to the volume-median drop radius  $a_0$ .

Example of interpretation: 30 percent of the liquid-water content of any cloud is contained in droplets which have a radius  $a_0$ . In the case of the B distribution, 20 percent of the liquid-water content is contained in droplets which have a radius smaller than the volume-median radius  $a_0$  by a ratio  $a/a_0 = 0.84$  and another 20 percent in droplets which have a radius larger than  $a_0$  by a ratio  $a/a_0 = 1.17$ . A similar interpretation applies to the remaining values.

TABLE III - SAMPLE CALCULATIONS FOR  $E_{\omega}$  FOR  
DISTRIBUTION B AND  $(K\varphi)_0 = 200$

(a)  $(1/K)_0$  for volume-median droplet size  
assigned value of 4.0;  $\varphi = 800$

Group	$a/a_0$	Percent water in each size group	K	$E_m$	E
1	0.56	5	0.079	-----	-----
2	.72	10	.130	-----	-----
3	.84	20	.177	0.003	0.0006
4	1.00	30	.250	.027	.0081
5	1.17	20	.343	.065	.0130
6	1.32	10	.435	.100	.0100
7	1.49	5	.555	.140	.0070

$$\Sigma = E_{\omega} = 0.0387$$


(b)  $(1/K)_0$  for volume-median droplet size  
assigned value of 1.0;  $\varphi = 200$

Group	$a/a_0$	Percent water in each size group	K	$E_m$	E
1	0.56	5	0.314	0.068	0.0034
2	.72	10	.518	.158	.0158
3	.84	20	.706	.225	.0450
4	1.00	30	1.000	.301	.0903
5	1.17	20	1.370	.384	.0768
6	1.32	10	1.740	.444	.0444
7	1.49	5	2.270	.515	.0258



$$\Sigma = E_{\omega} = 0.302$$

TABLE IV - VALUES OF WEIGHTED COLLECTION EFFICIENCY  $E_w$  FOR DROPLET-SIZE DISTRIBUTIONS A, B, C, D, AND E

$(1/K)_o$	$E_w$									
	$(K\phi)_o = 0$					$(K\phi)_o = 200$				
	A	B	C	D	E	A	B	C	D	E
4	0.051	0.069	0.085	0.107	0.126	0.027	0.039	0.050	0.066	0.083
2	.205	.204	.211	.225	.241	.135	.138	.146	.165	.182
1	.380	.374	.373	.379	.384	.298	.302	.306	.315	.319
.5	.566	.555	.549	.542	.536	.493	.486	.482	.480	.477
.2	.789	.768	.750	.732	.713	.761	.740	.721	.703	.686
.1	.885	.870	.854	.836	.815	.874	.859	.846	.826	.805
.05	.932	.925	.918	.898	.885	.925	.919	.910	.901	.878
.02	.963	.961	.957	.951	.940	.960	.959	.955	.948	.938
.01	.978	.976	.977	.972	.965	.976	.975	.976	.971	.963
$(K\phi)_o = 1000$					$(K\phi)_o = 3000$					
4	0.019	0.029	0.038	0.050	0.065	0.013	0.020	0.027	0.039	0.048
2	.109	.109	.122	.138	.154	.085	.090	.100	.111	.130
1	.251	.252	.259	.271	.283	.218	.225	.235	.244	.251
.5	.460	.452	.423	.447	.447	.409	.416	.410	.415	.413
.2	.714	.697	.677	.661	.643	.687	.668	.652	.641	.623
.1	.830	.816	.800	.783	.763	.815	.797	.785	.766	.746
.05	.908	.899	.892	.876	.862	.884	.878	.867	.855	.839
.02	.953	.953	.949	.943	.933	.945	.940	.938	.921	.918
.01	.971	.972	.973	.967	.962	.968	.966	.970	.964	.954
$(K\phi)_o = 10,000$										
4	0.008	0.013	0.017	0.023	0.034					
2	.057	.060	.072	.083	.092					
1	.157	.163	.172	.188	.202					
.5	.350	.356	.357	.362	.368					
.2	.645	.630	.615	.599	.591					
.1	.778	.764	.748	.731	.713					
.05	.865	.857	.849	.830	.816					
.02	.920	.920	.918	.909	.899					
.01	.952	.950	.955	.946	.939					



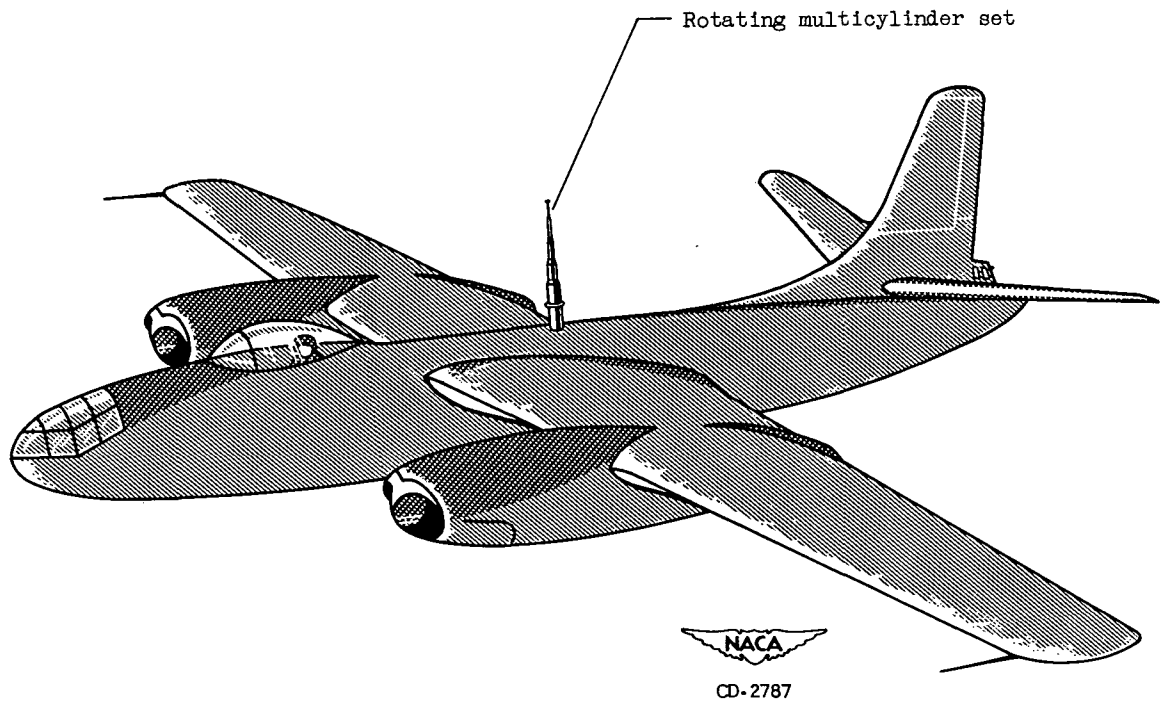


Figure 1. - Rotating multicylinder set extended through top of airplane fuselage.

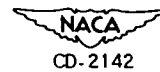
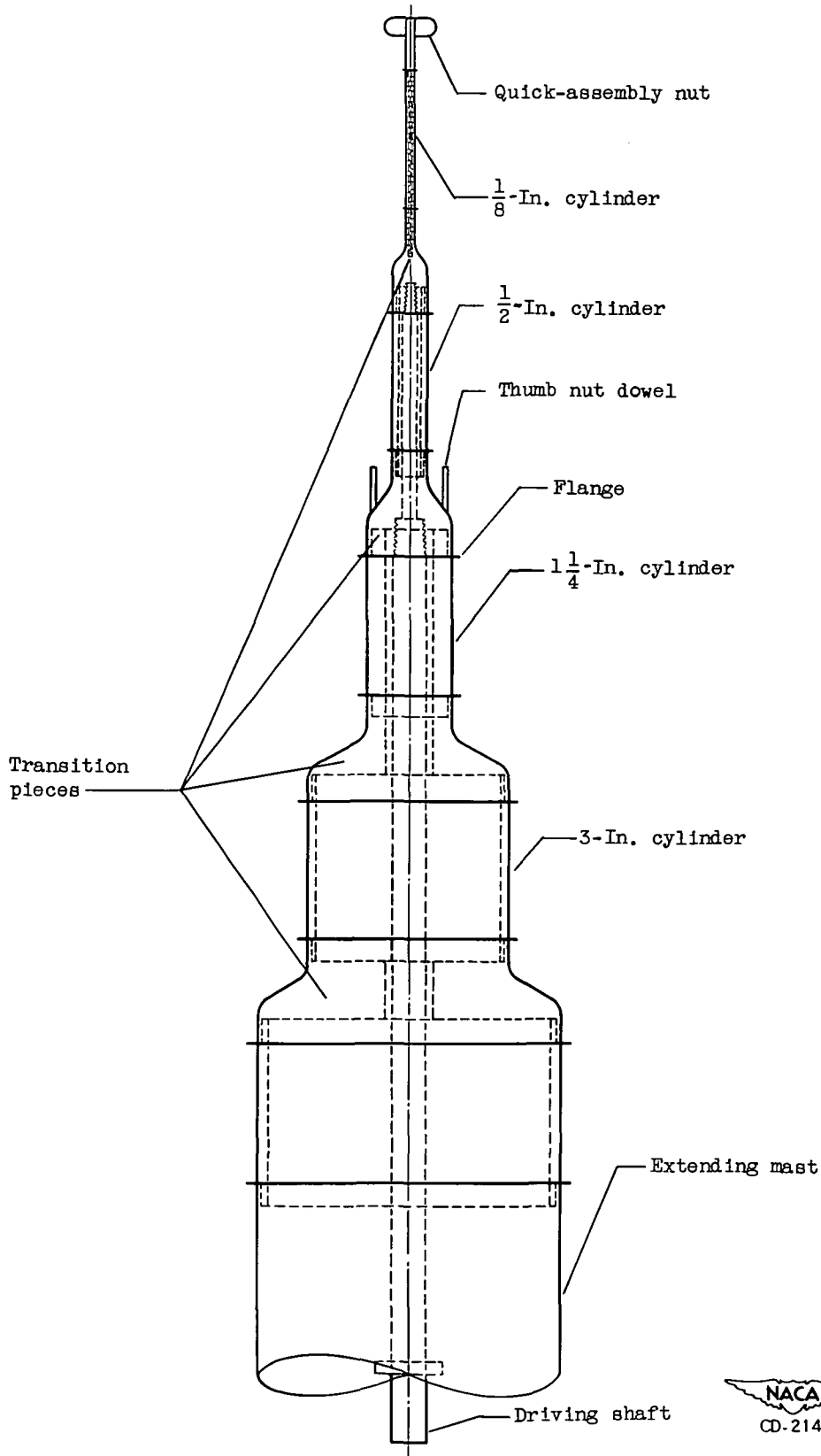


Figure 2. - Assembled set of rotating multicylinders.

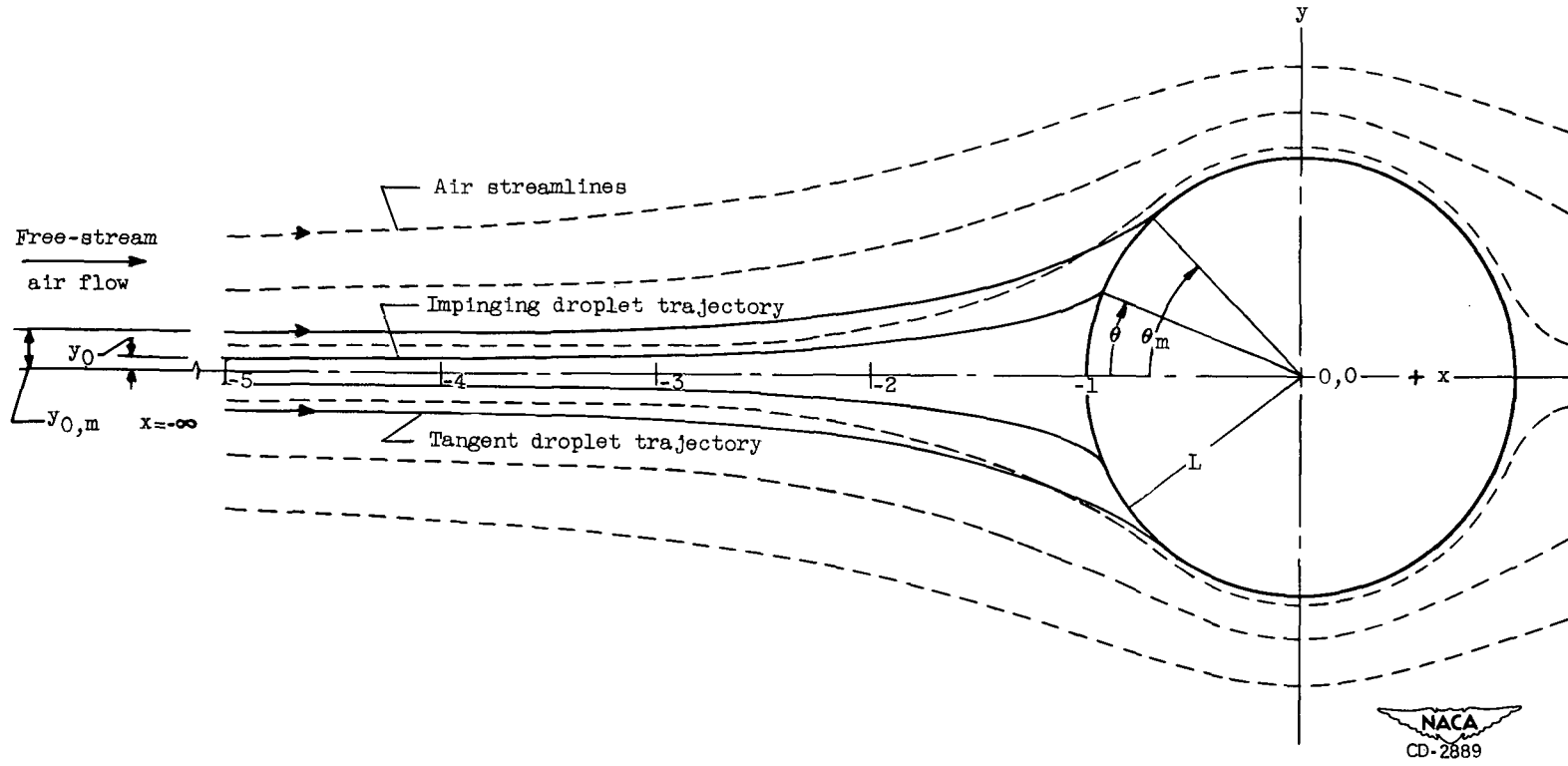


Figure 3. - Air streamlines and droplet trajectories with respect to right circular cylinder.

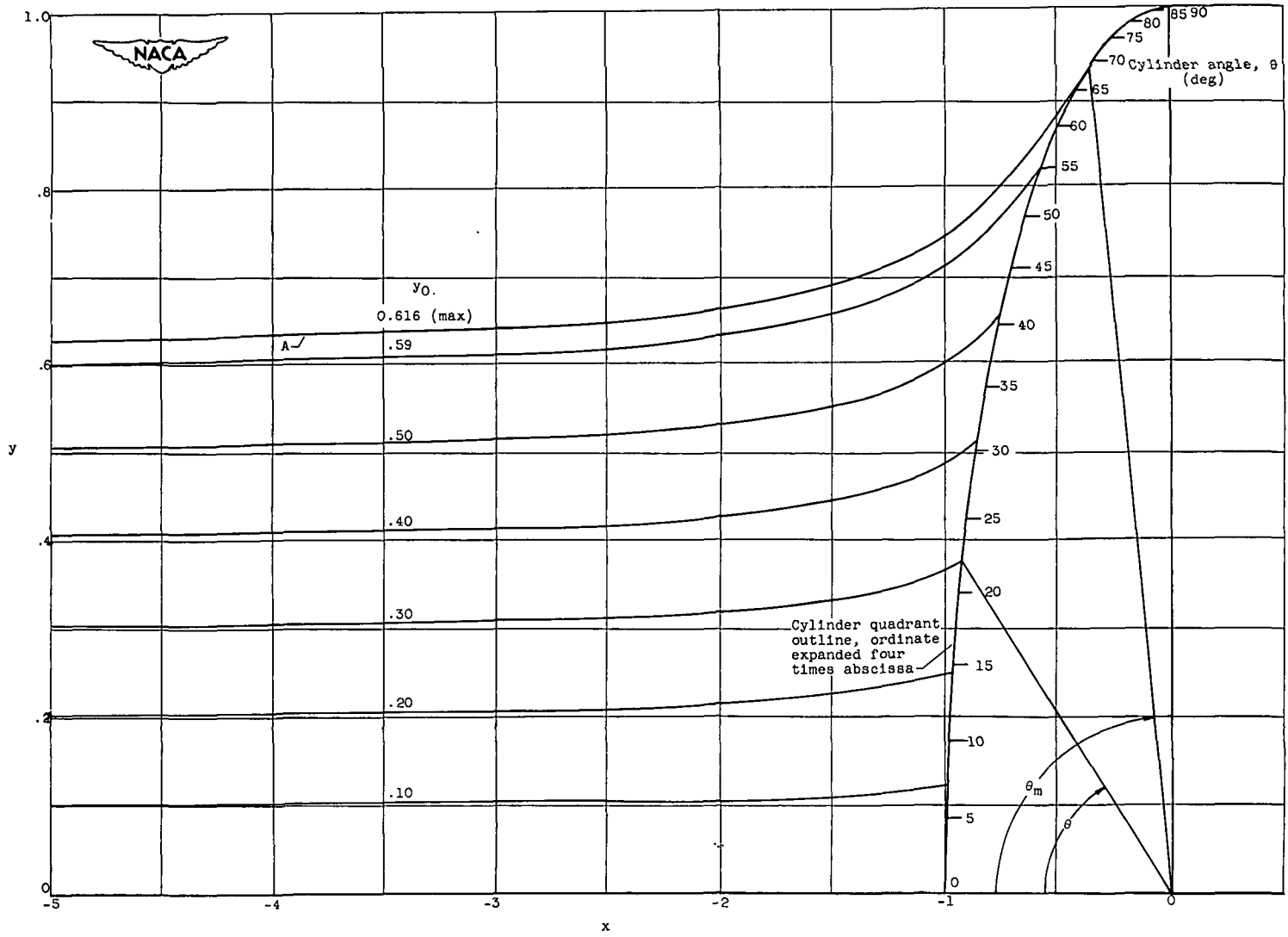


Figure 4. - Trajectories of droplets impinging on cylinder. Free-stream Reynolds number, 63.246; inertia parameter, 4;  $\varphi$ , 1000.

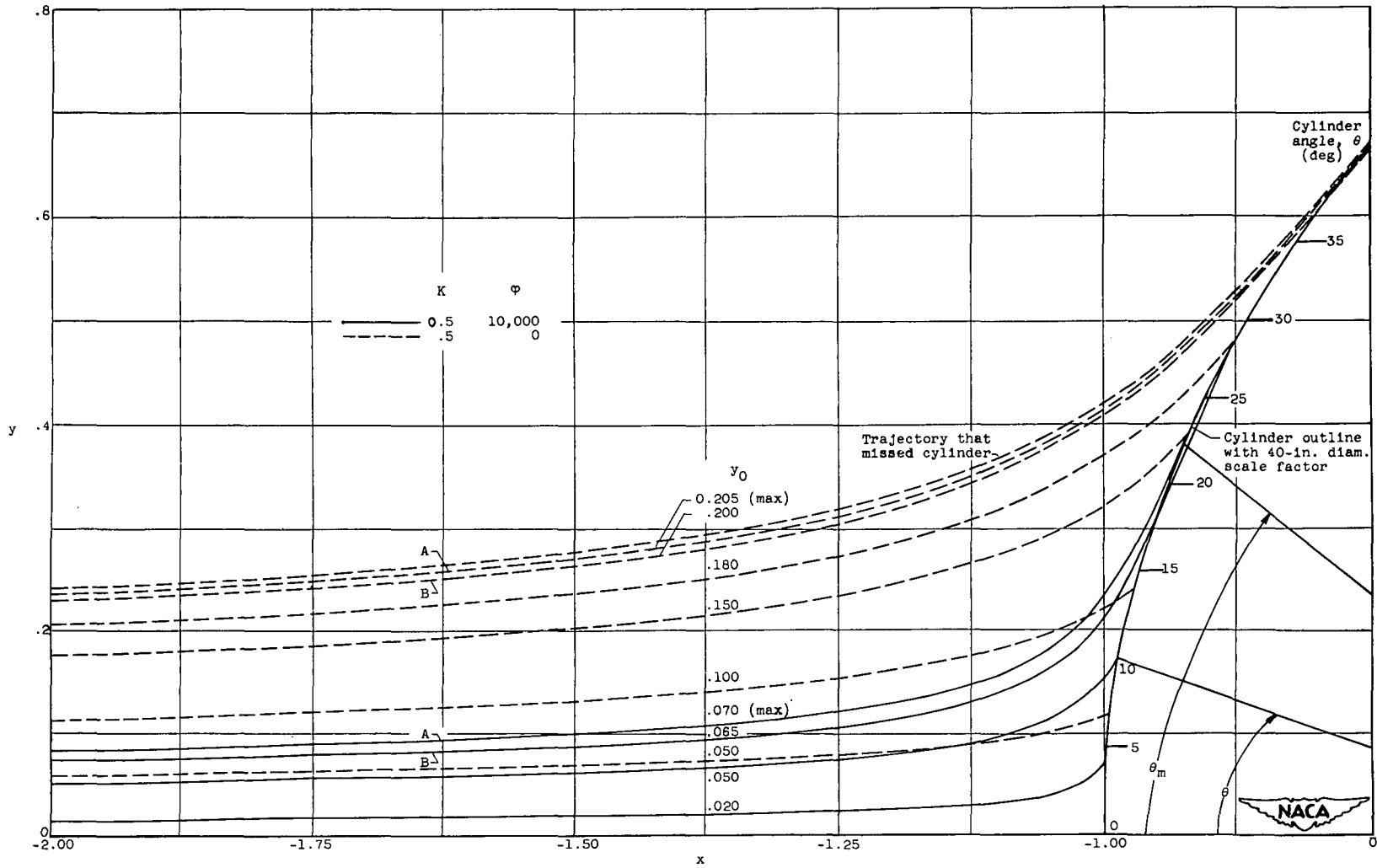


Figure 5. - Trajectories of droplets with low inertia.

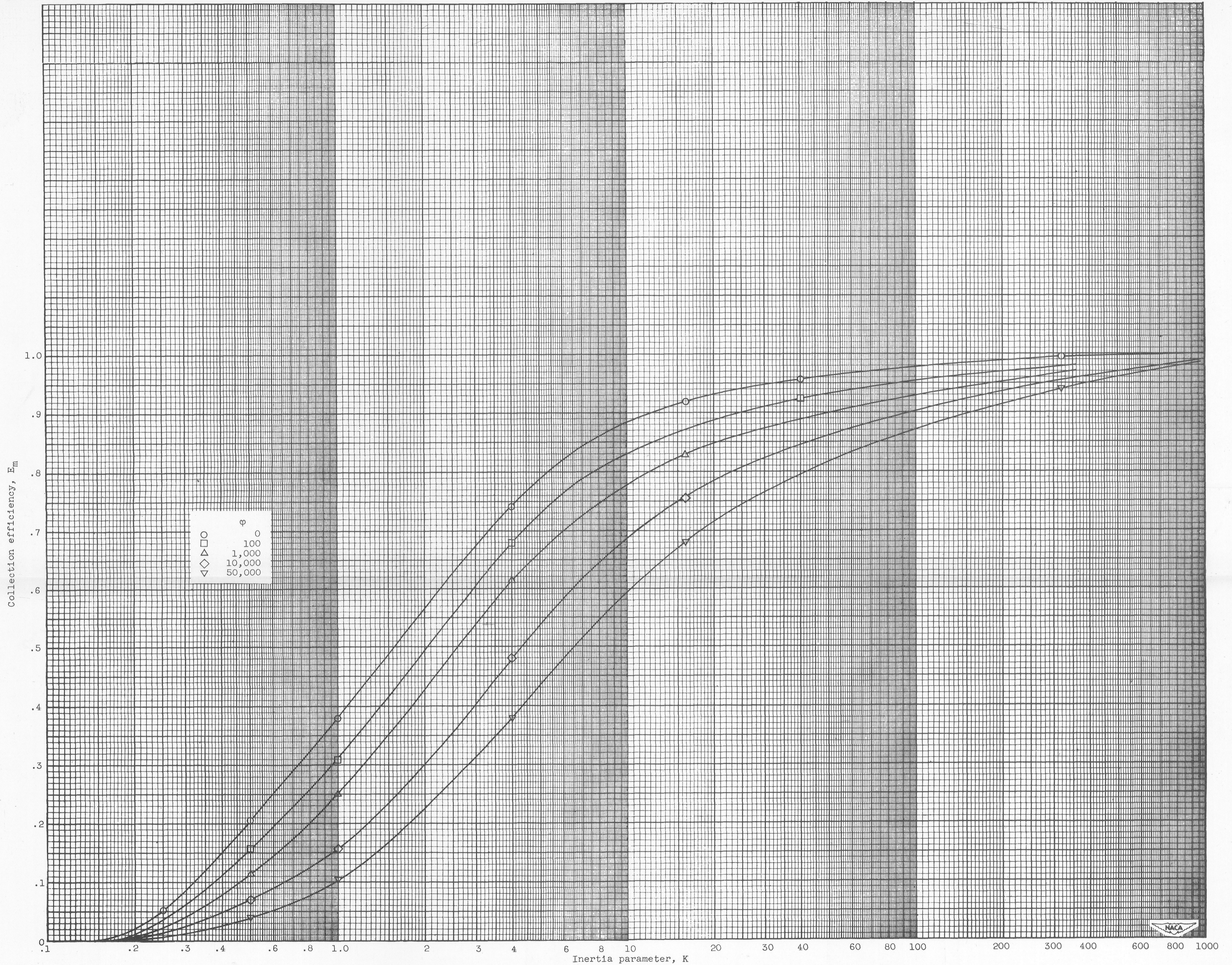


Figure 6. - Cylinder collection efficiency.



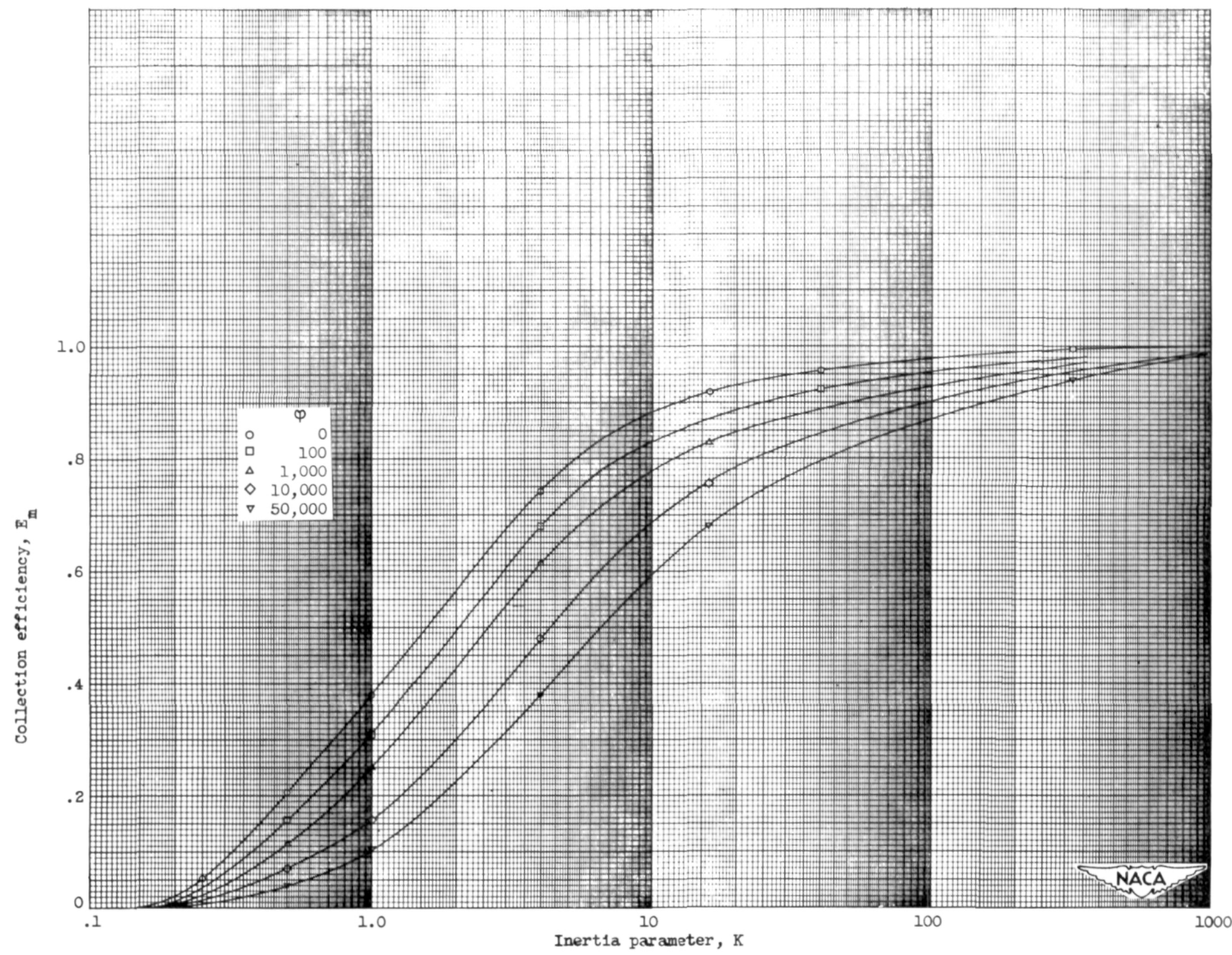


Figure 6. - Cylinder collection efficiency. (A 17- by 21-in. print of this fig. is attached.)

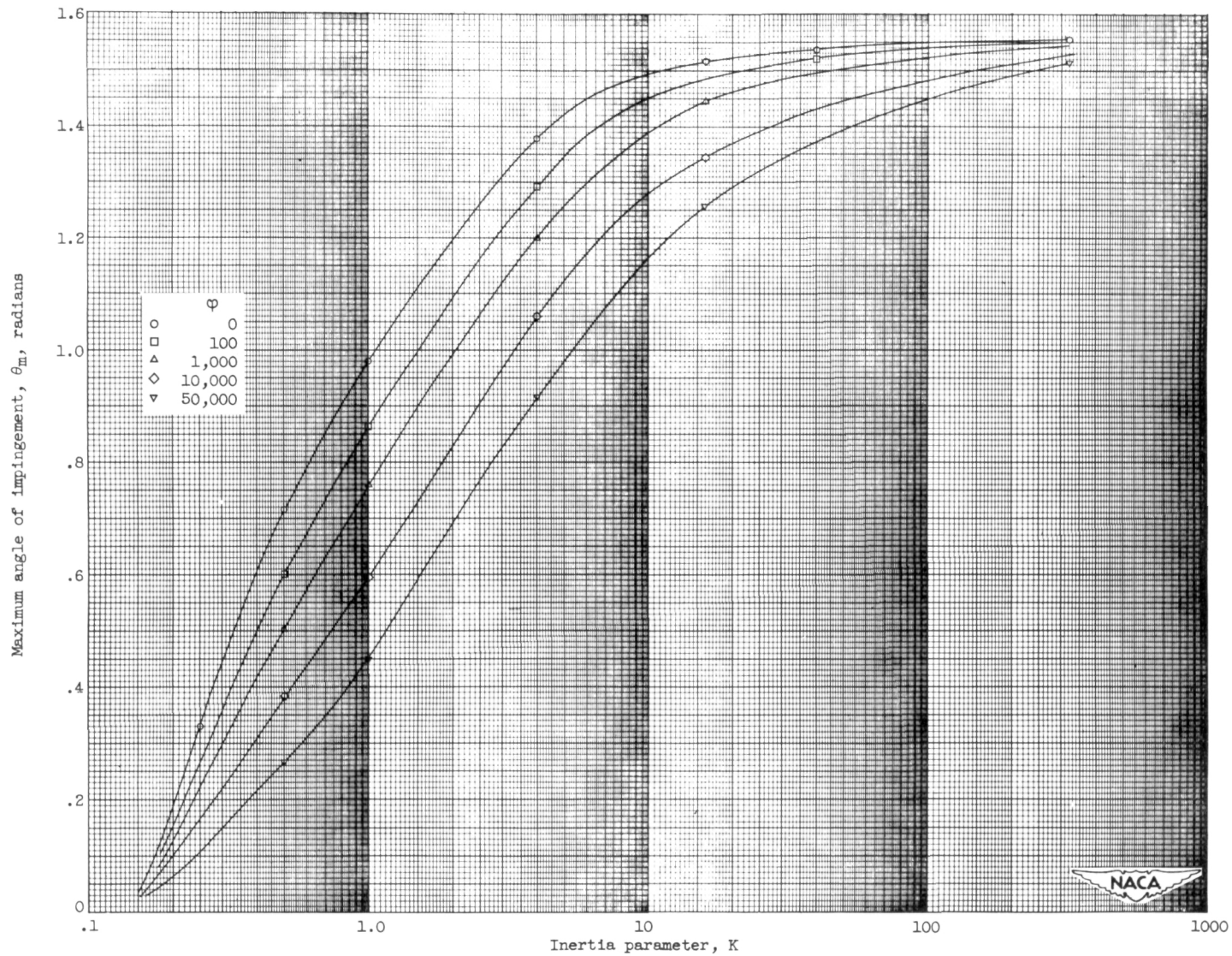


Figure 7. - Maximum angle of impingement on cylinder. (A 17- by 21-in. print of this fig. is attached.)



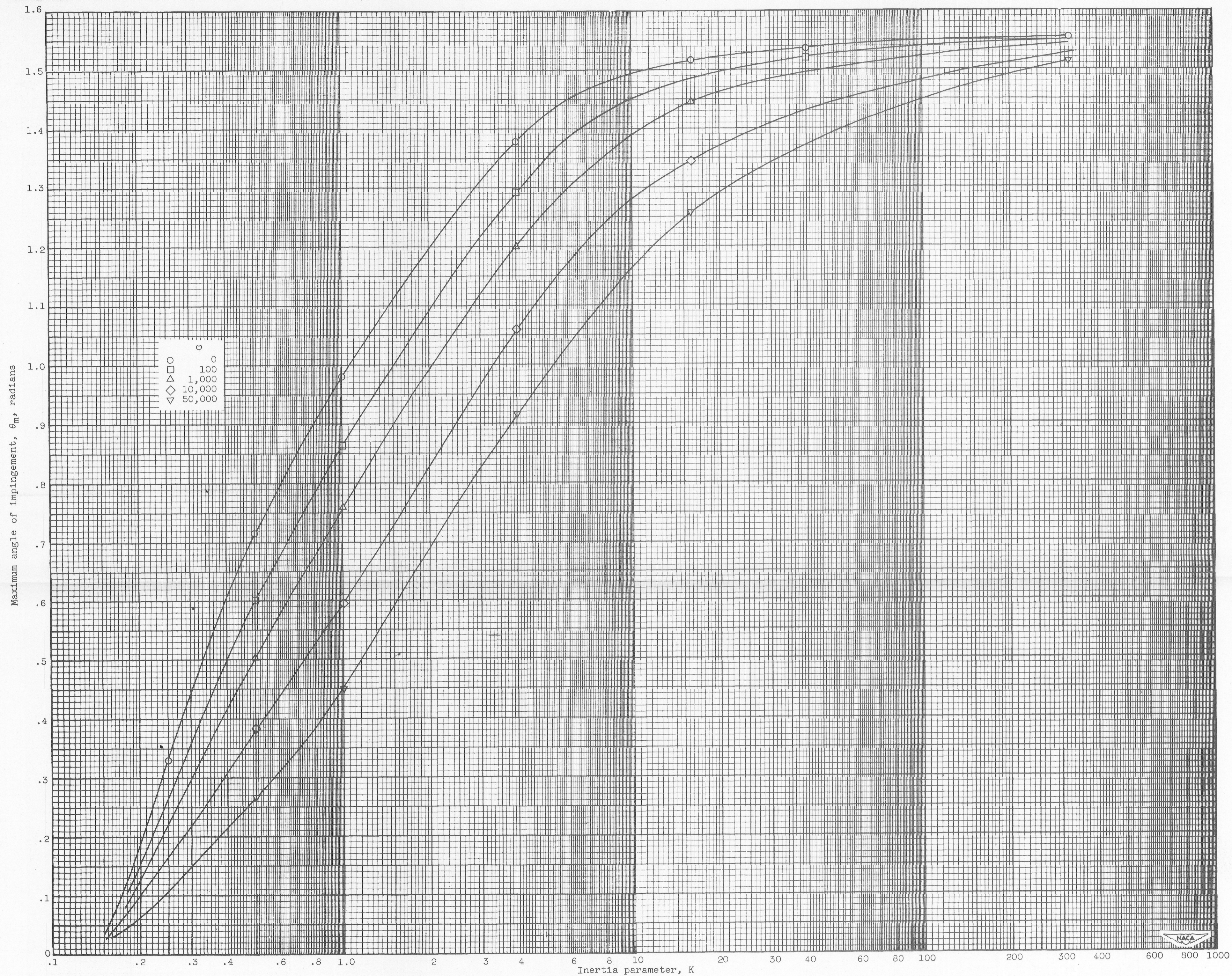


Figure 7. - Maximum angle of impingement on cylinder.



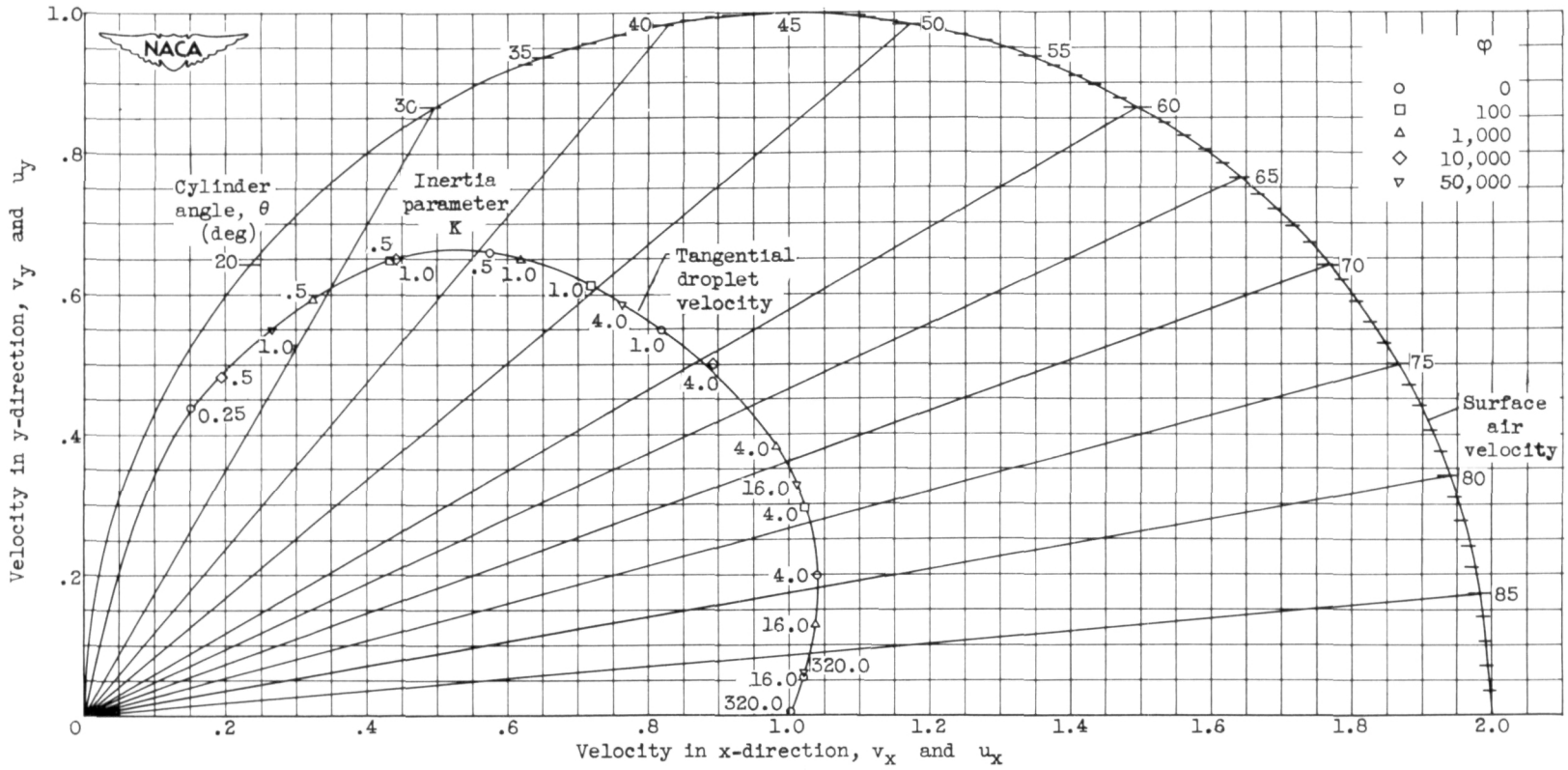


Figure 8. - Tangential-velocity hodograph for air and droplets at surface of cylinder.

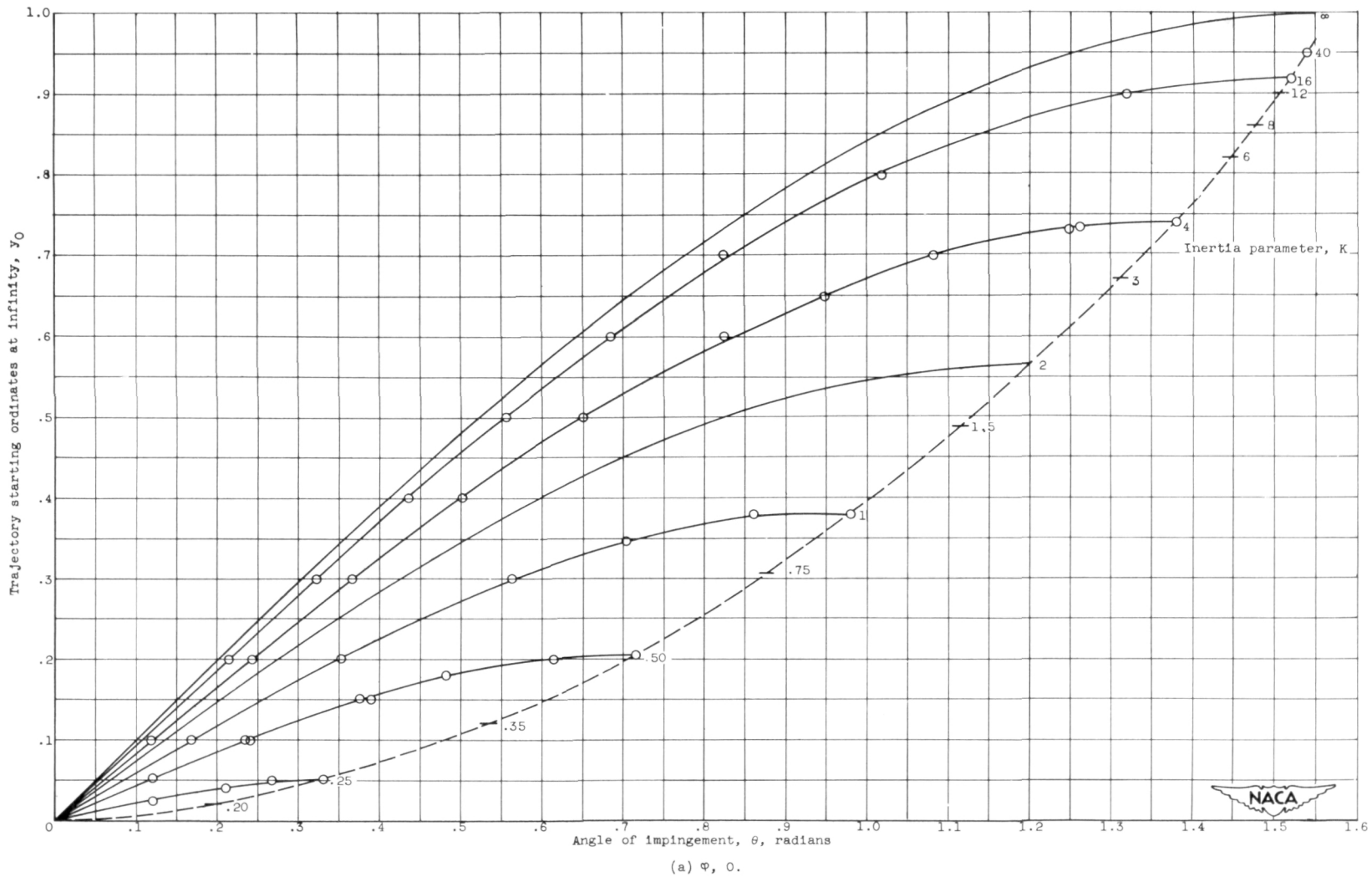
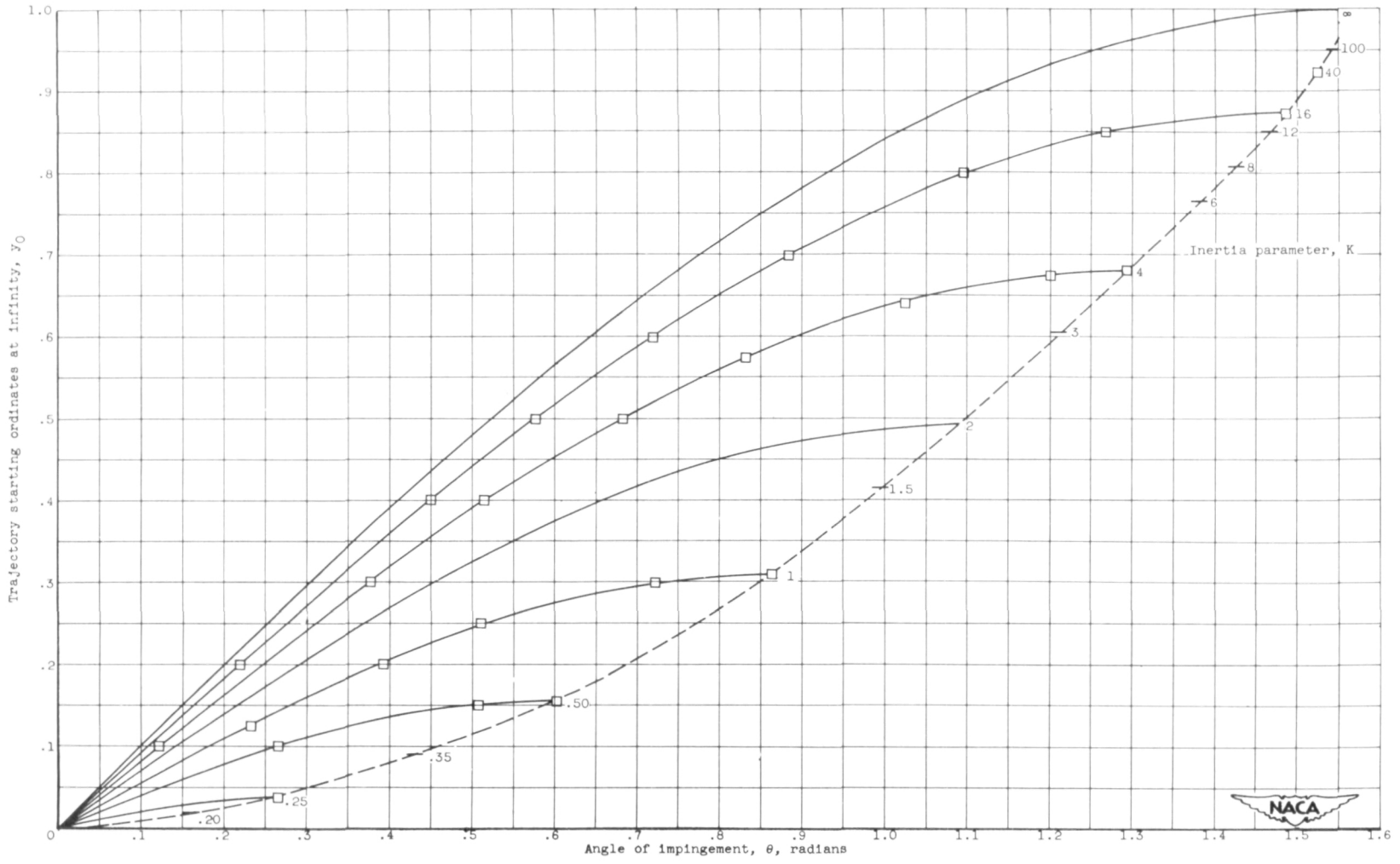


Figure 9. - Trajectory starting ordinates as function of angle of impingement.





(b)  $\Phi$ , 100.  
Figure 9. - Continued. Trajectory starting ordinates as function of angle of impingement.



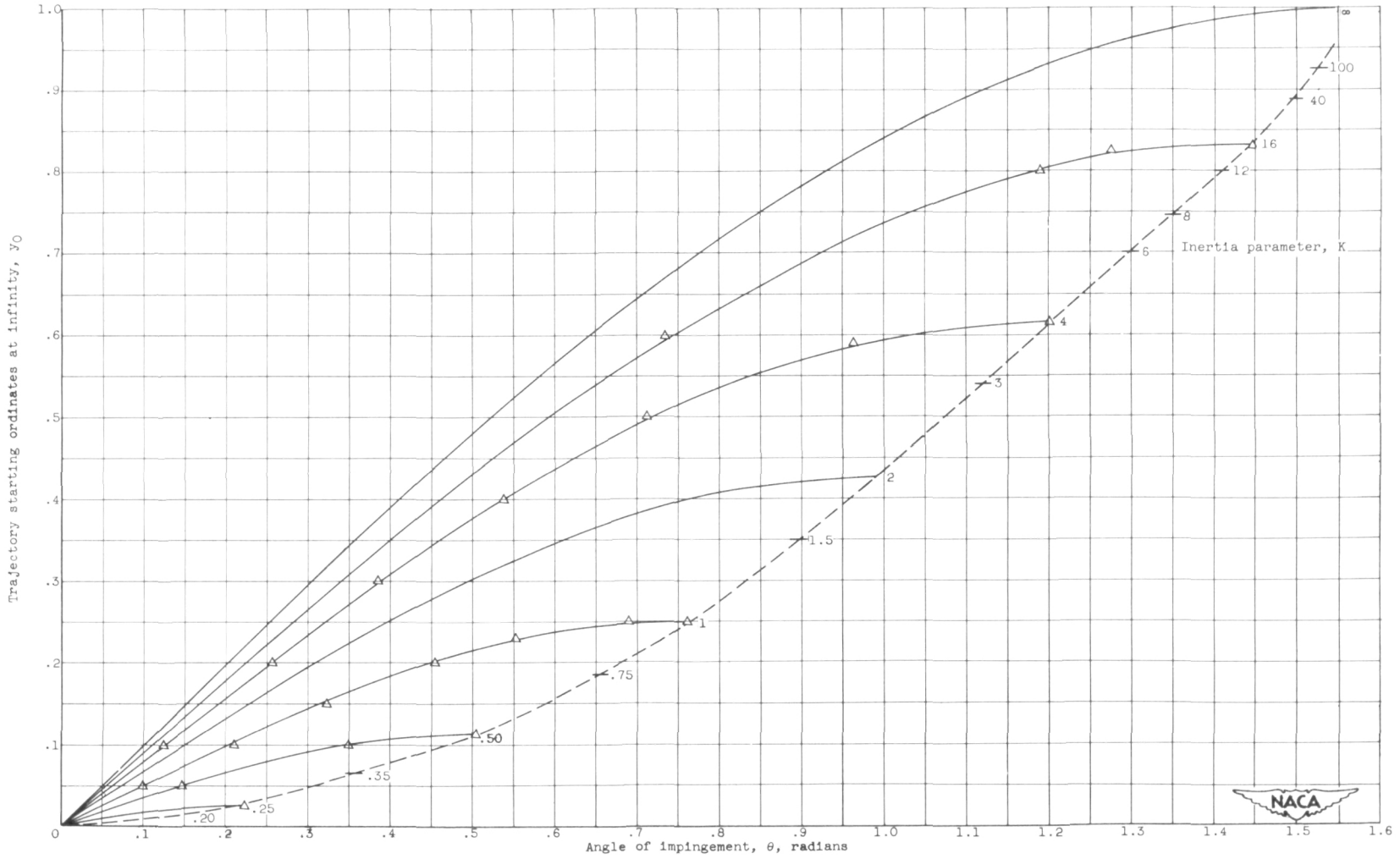


Figure 9. - Continued. Trajectory starting ordinates as function of angle of impingement.

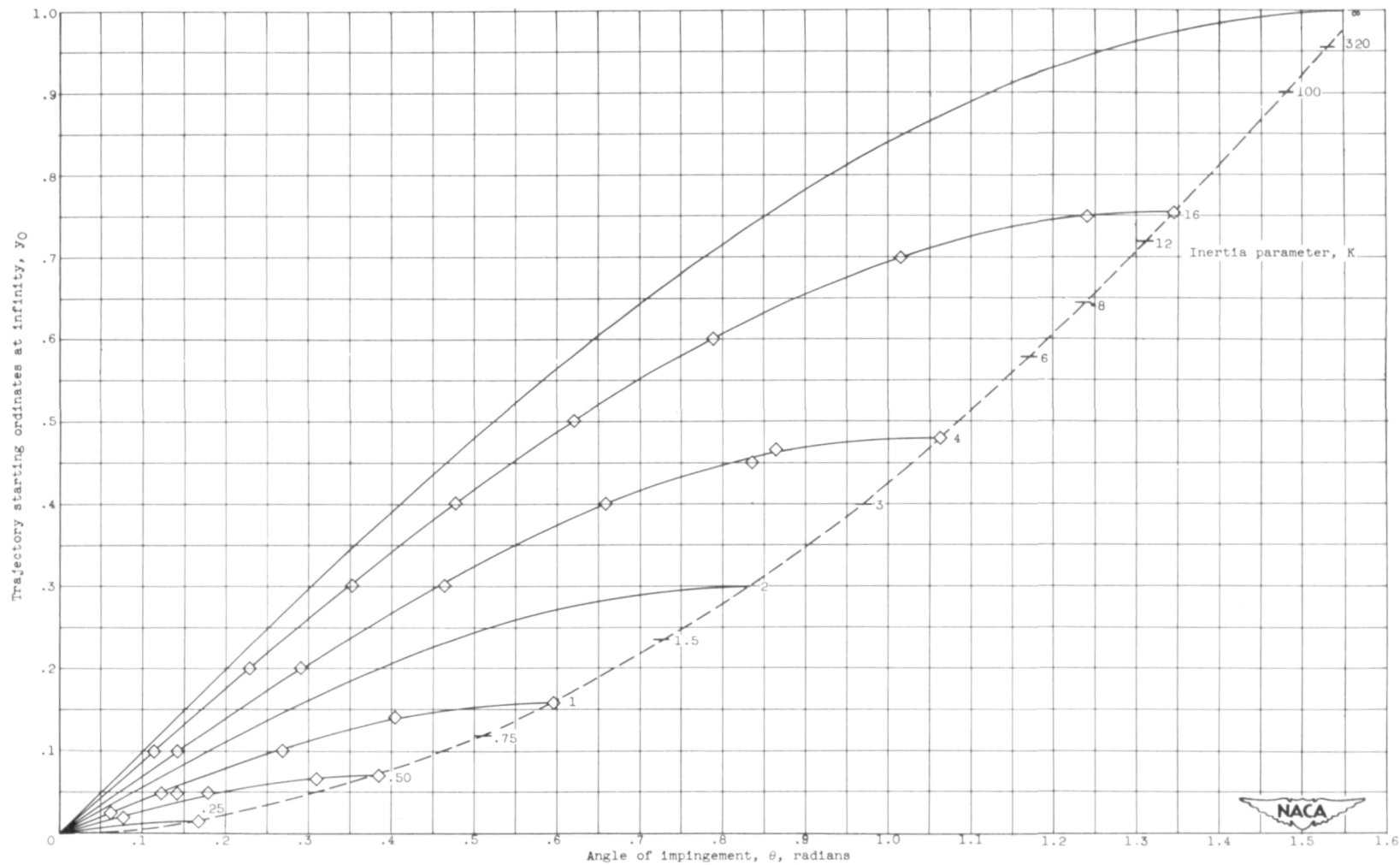


Figure 9. - Continued. Trajectory starting ordinates as function of angle of impingement

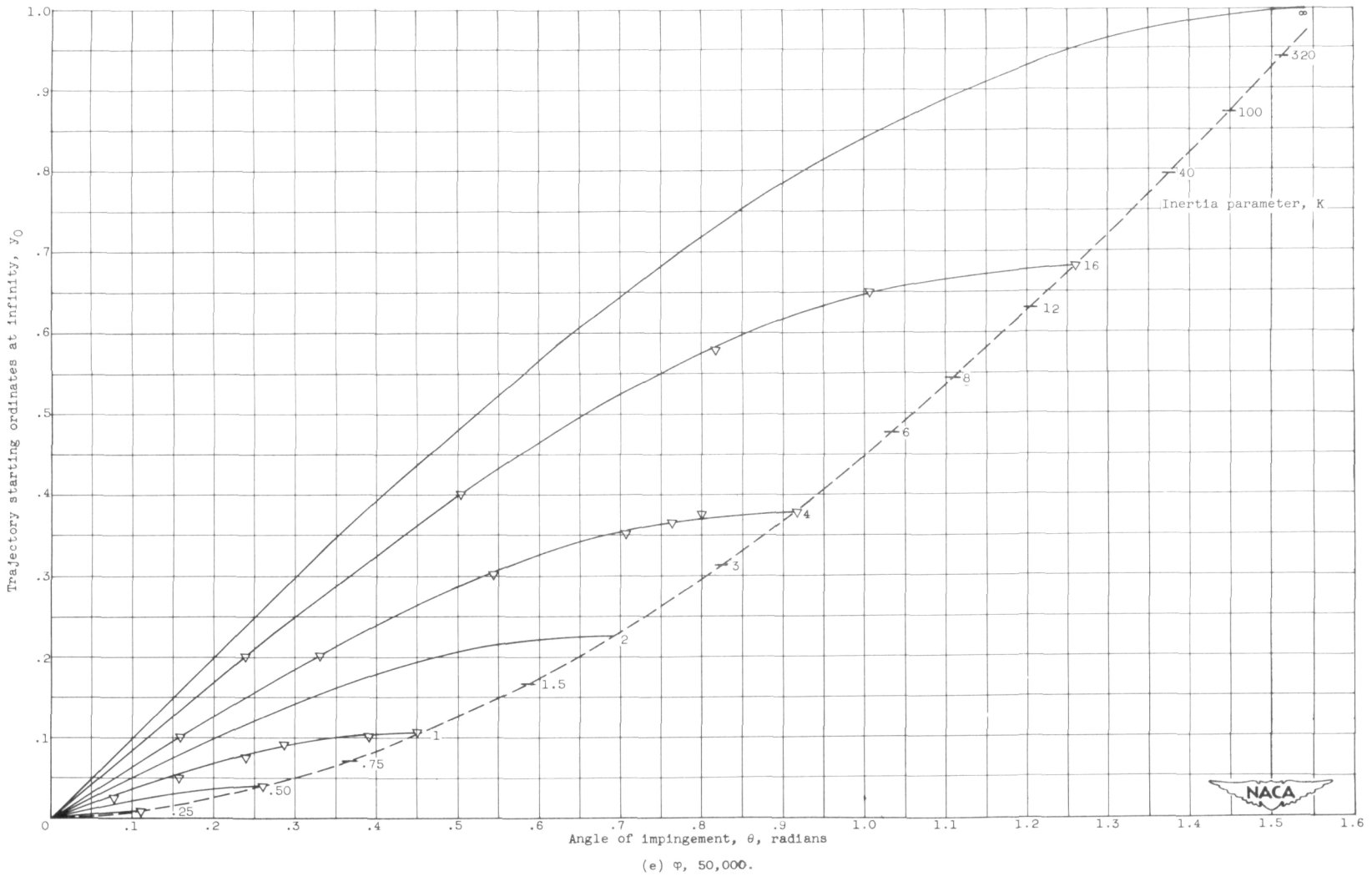
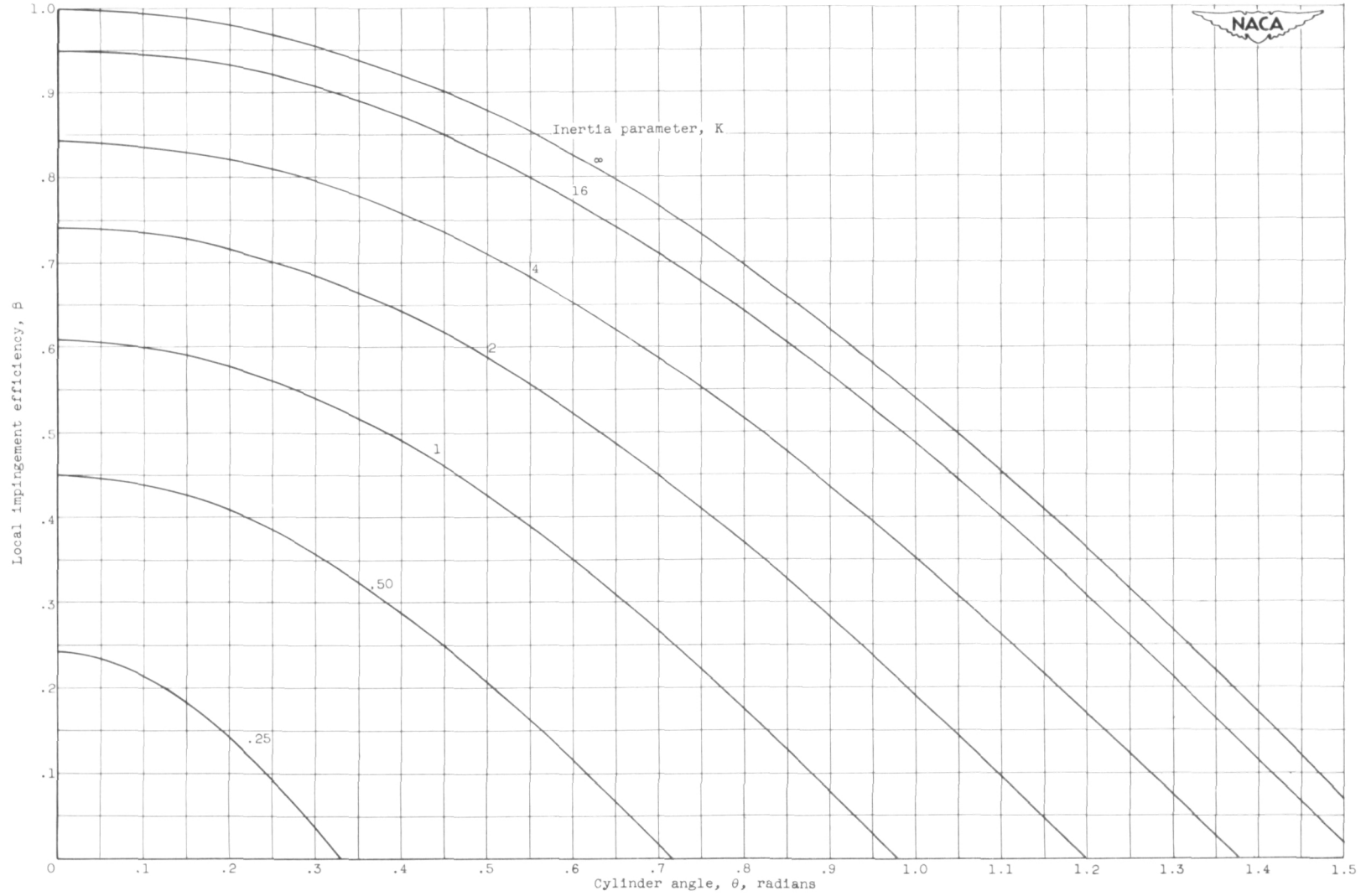


Figure 9. - Concluded. Trajectory starting ordinates as function of angle of impingement.



(a)  $\varphi, 0.$

Figure 10. - Local impingement efficiency as function of cylinder angle.



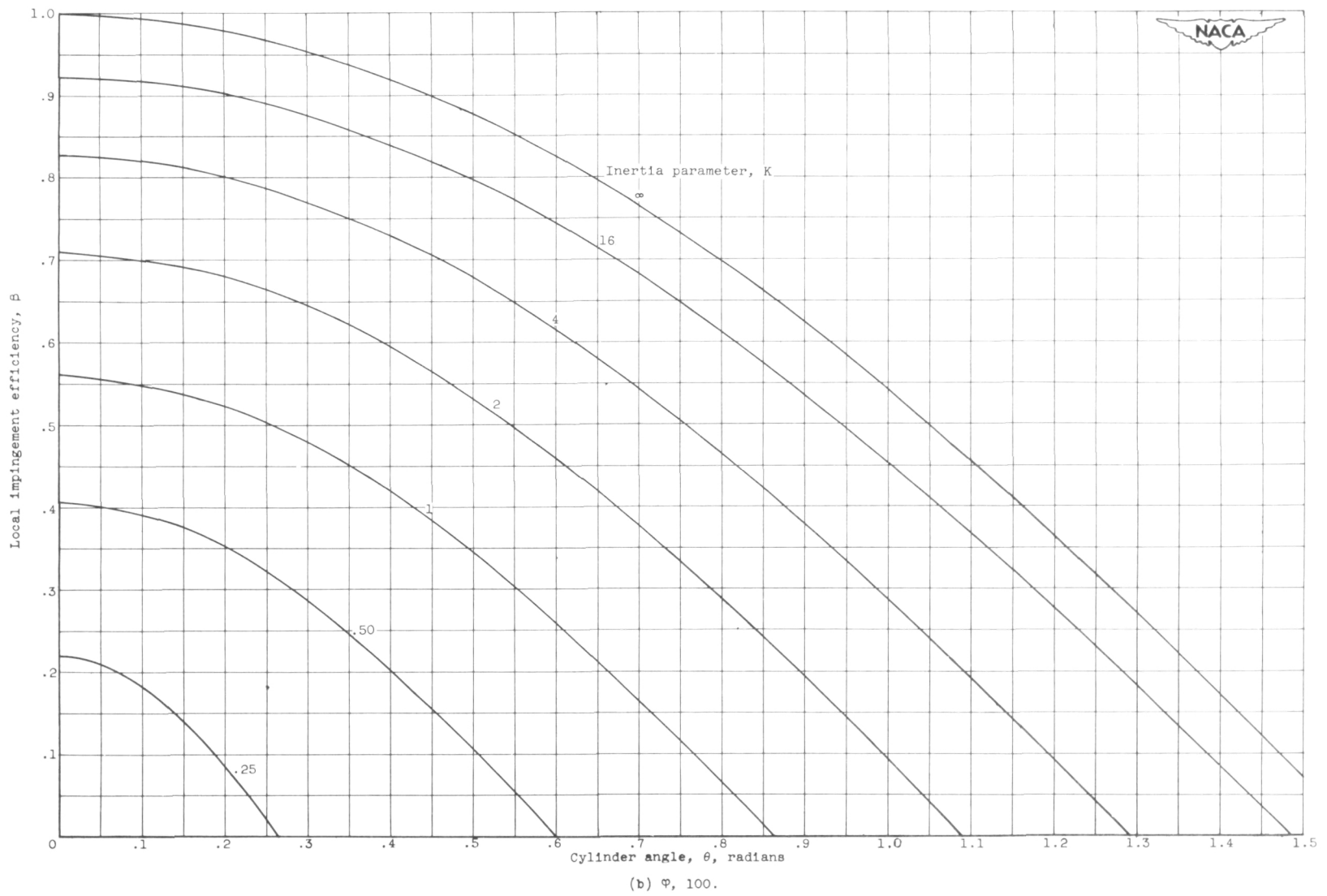


Figure 10. - Continued. Local impingement efficiency as function of cylinder angle.

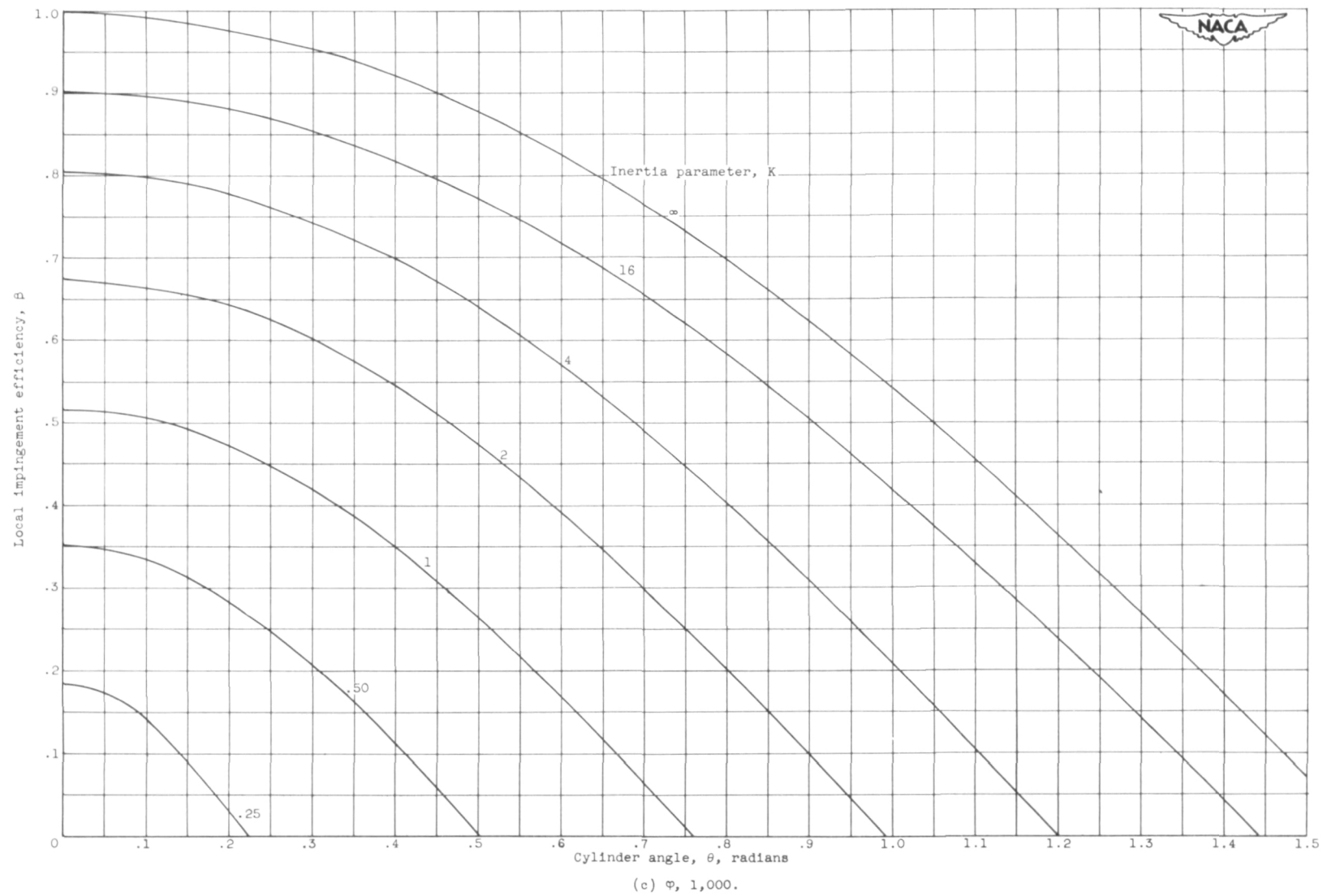


Figure 10. - Continued. Local impingement efficiency as function of cylinder angle.

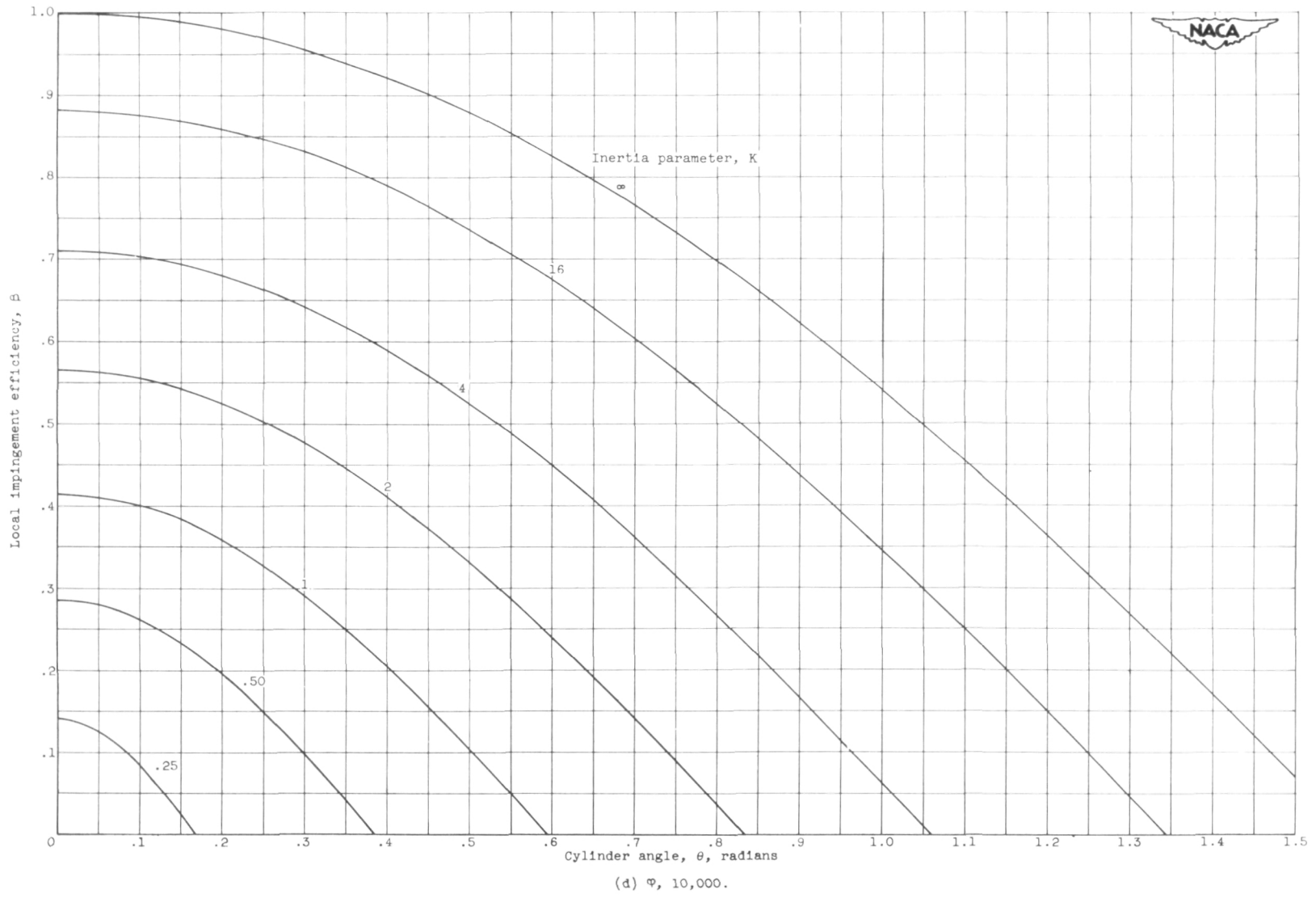


Figure 10. - Continued. Local impingement efficiency as function of cylinder angle.

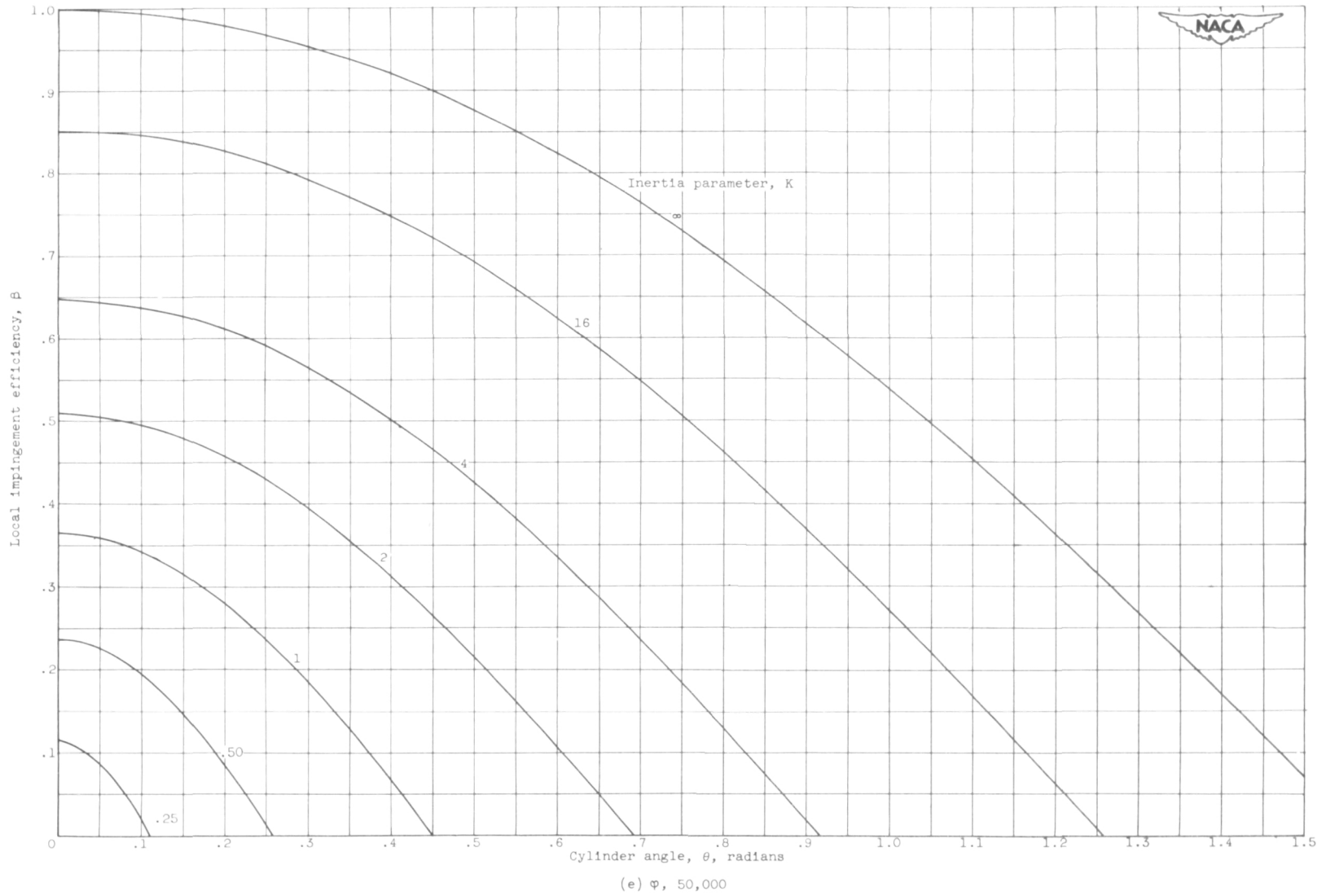


Figure 10. - Concluded. Local impingement efficiency as function of cylinder angle.

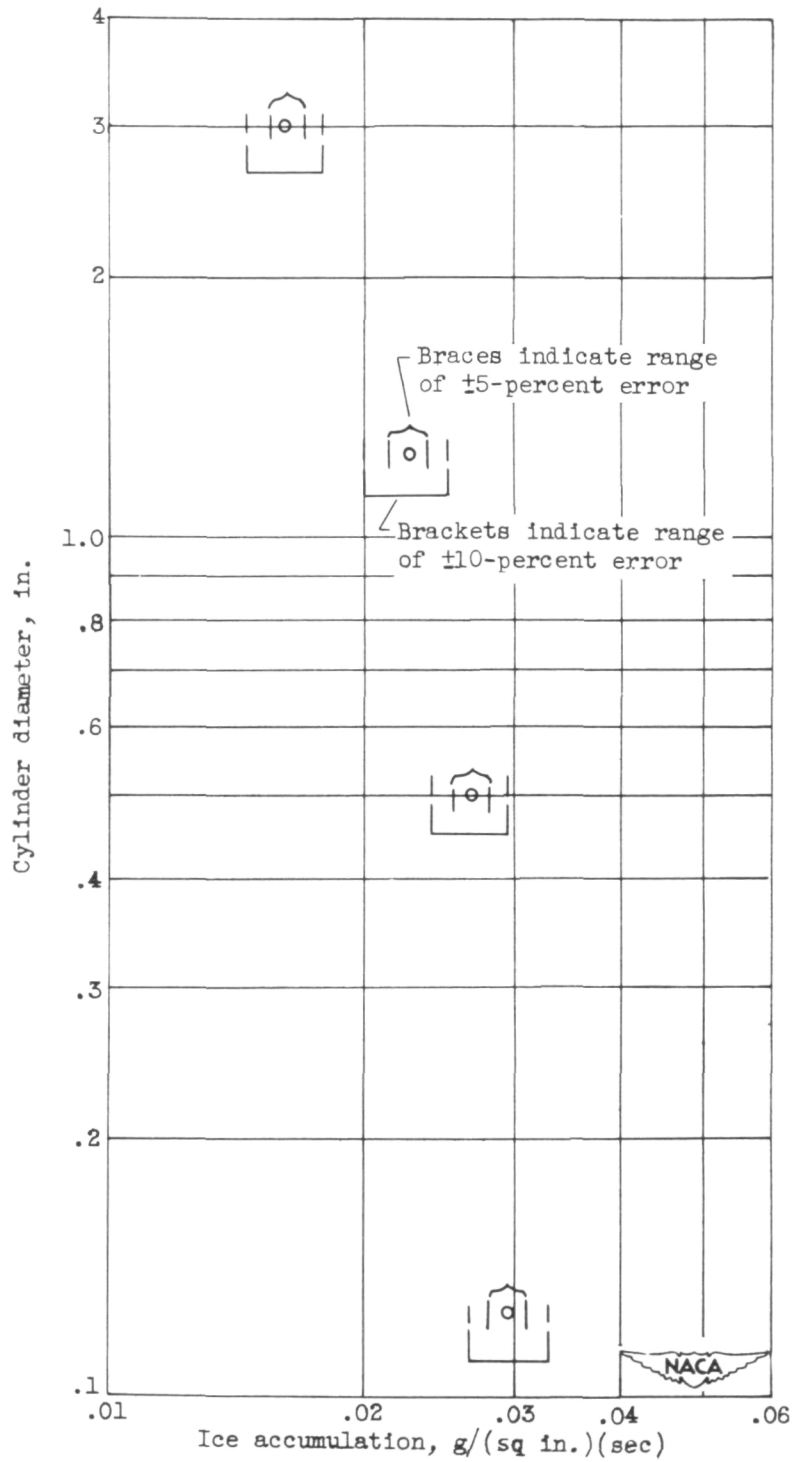


Figure 11. - Ice accumulation on set of cylinders. Speed, 200 miles per hour; air viscosity,  $3.436 \times 10^{-7}$  slugs per foot-second; altitude, 10,000 feet.

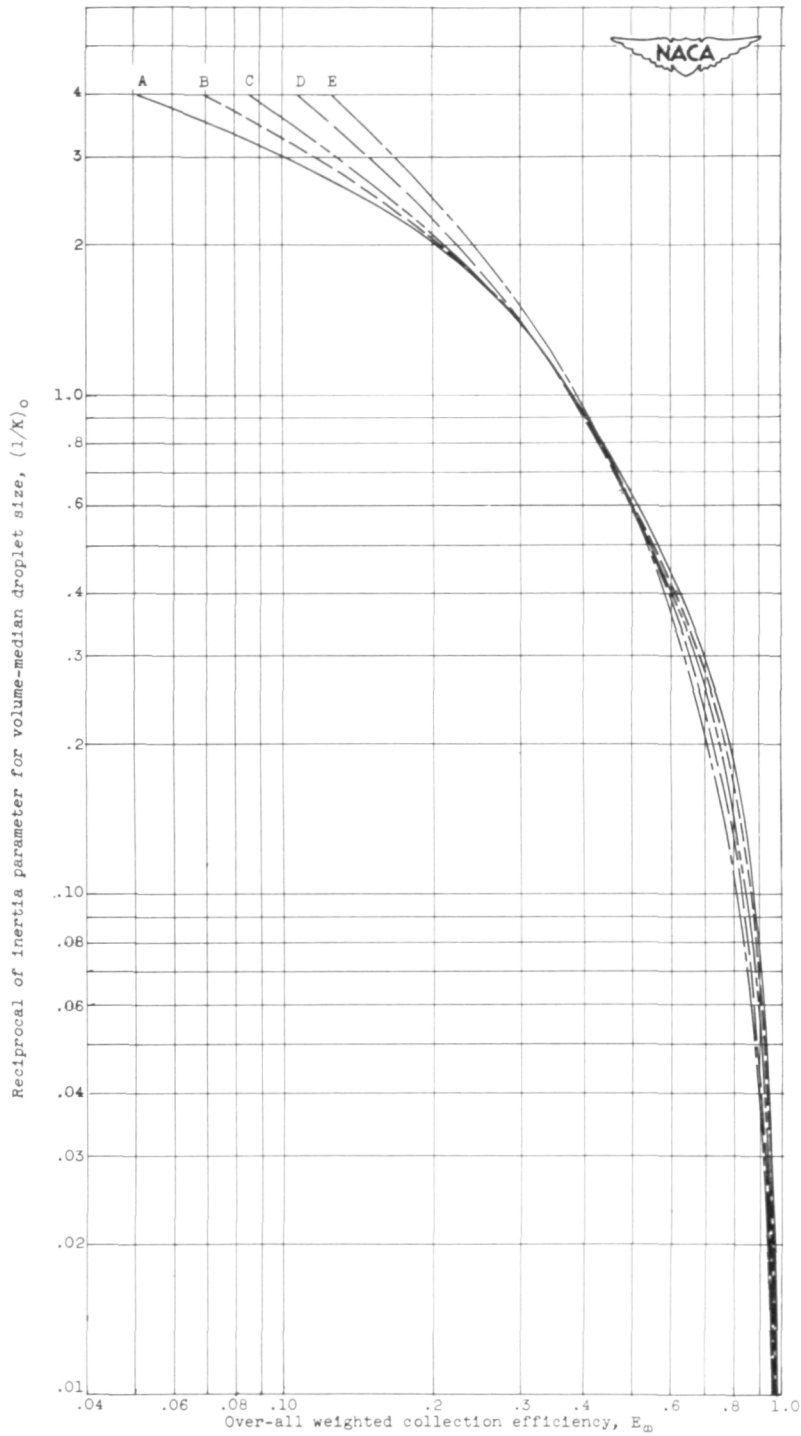


Figure 12. - Over-all weighted collection efficiency plotted against reciprocal of inertia parameter for volume-median droplet size for five cloud-droplet-size distributions.

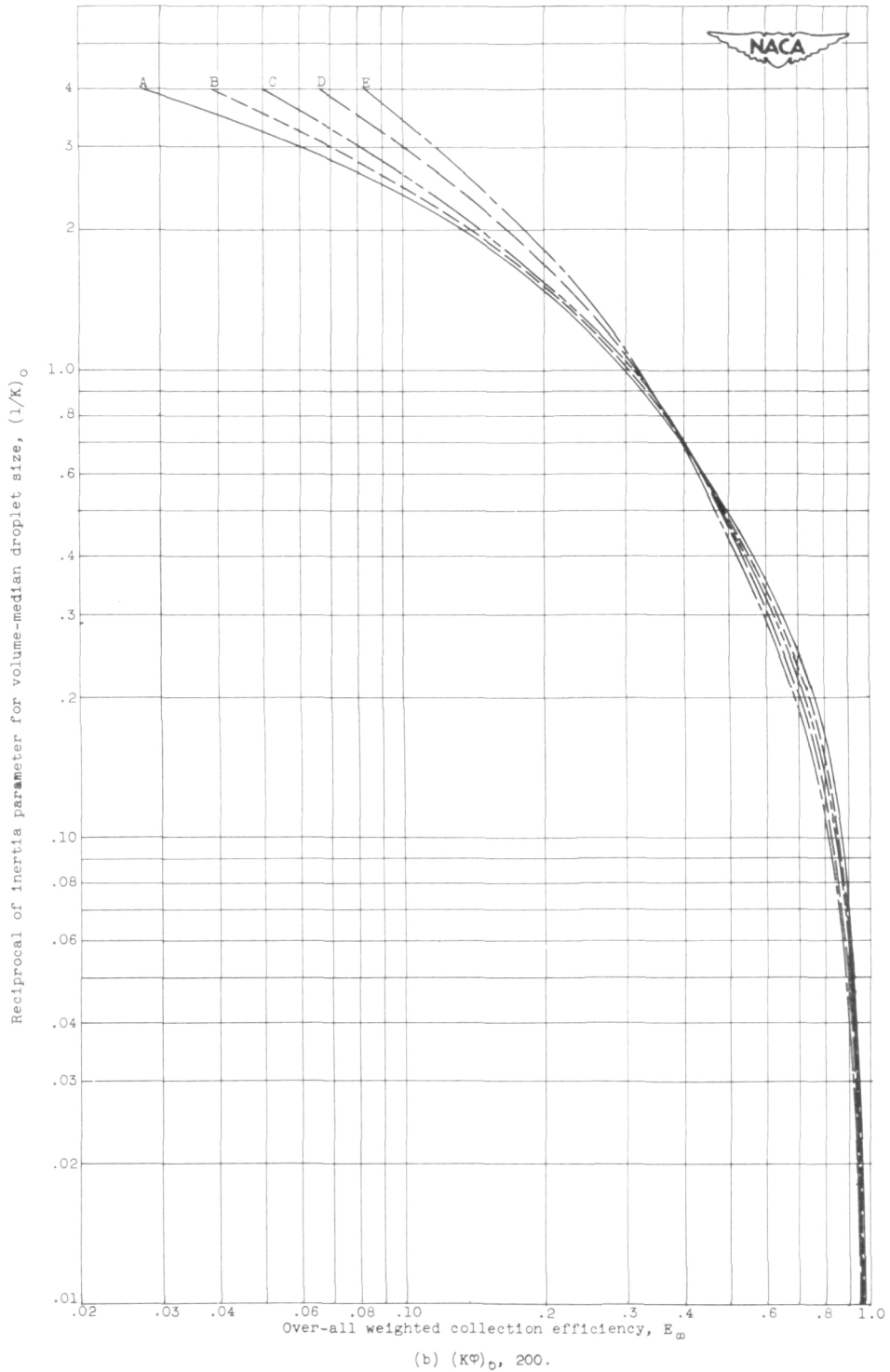


Figure 12. - Continued. Over-all weighted collection efficiency plotted against reciprocal of inertia parameter for volume-median droplet size for five cloud-droplet-size distributions.

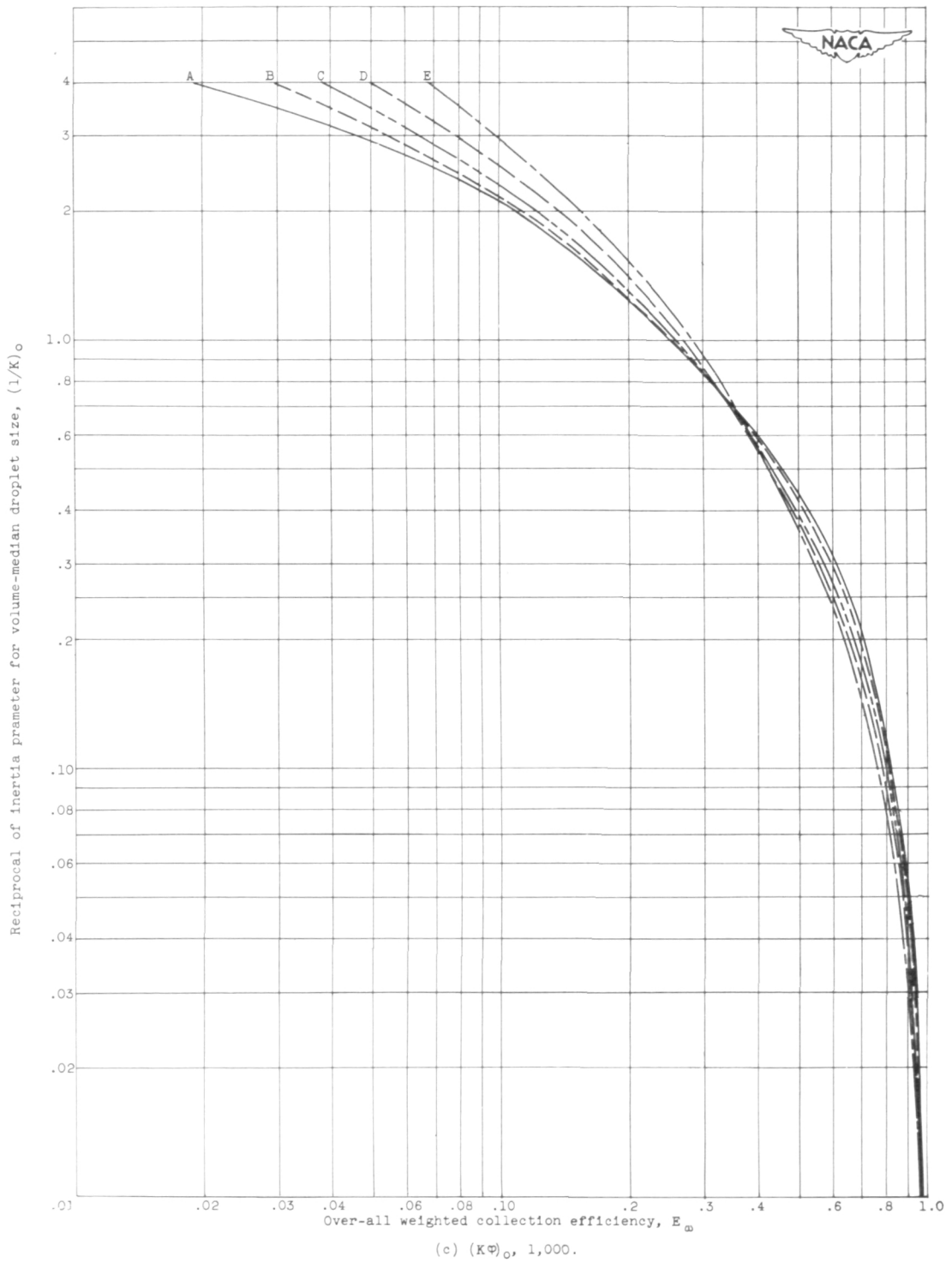
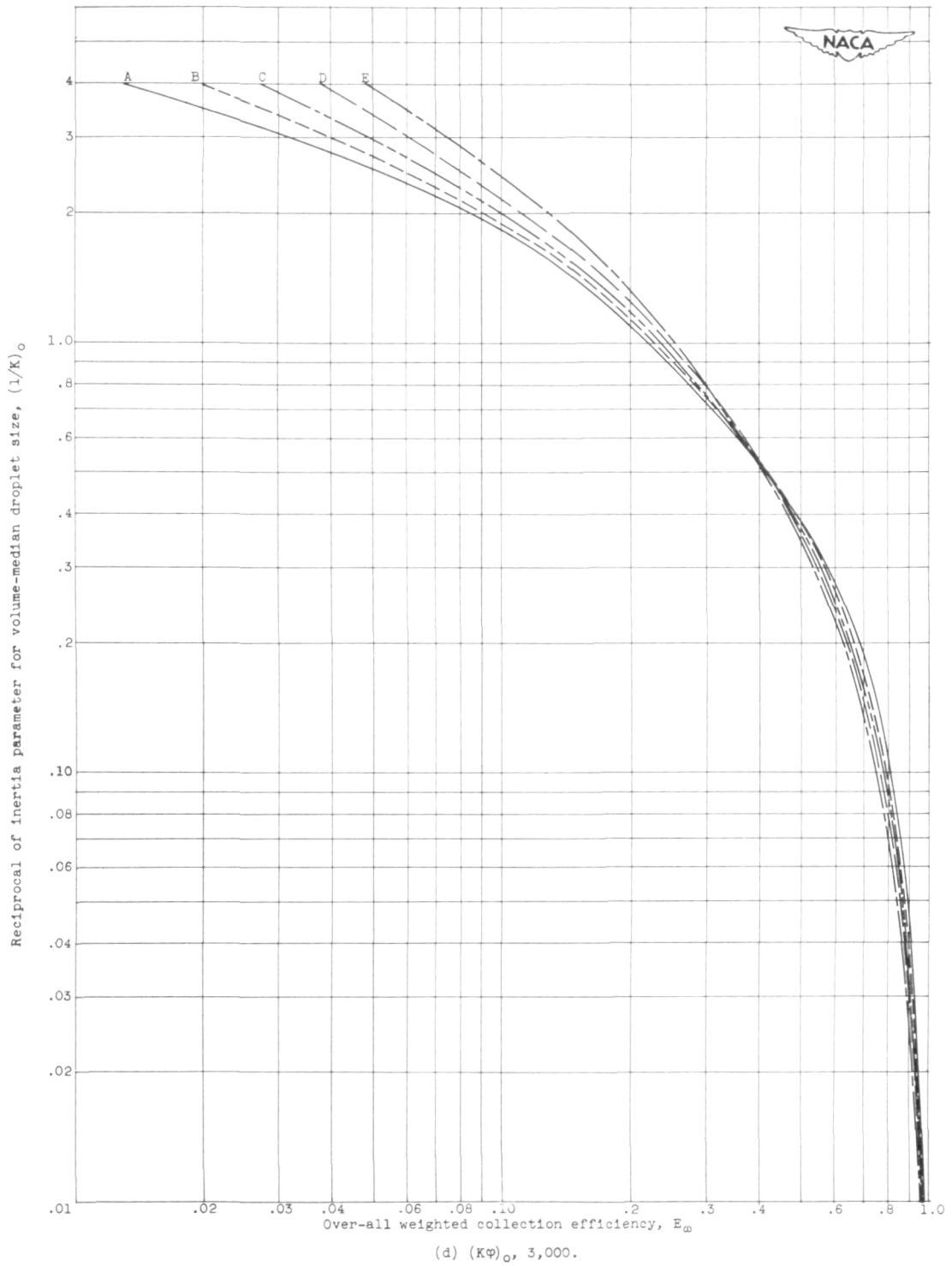


Figure 12. - Continued. Over-all weighted collection efficiency plotted against reciprocal of inertia parameter for volume-median droplet size for five cloud-droplet-size distributions.





(d)  $(K\Phi)_0, 3,000$ .

Figure 12. - Continued. Over-all weighted collection efficiency plotted against reciprocal of inertia parameter for volume-median droplet size for five cloud-droplet-size distributions.

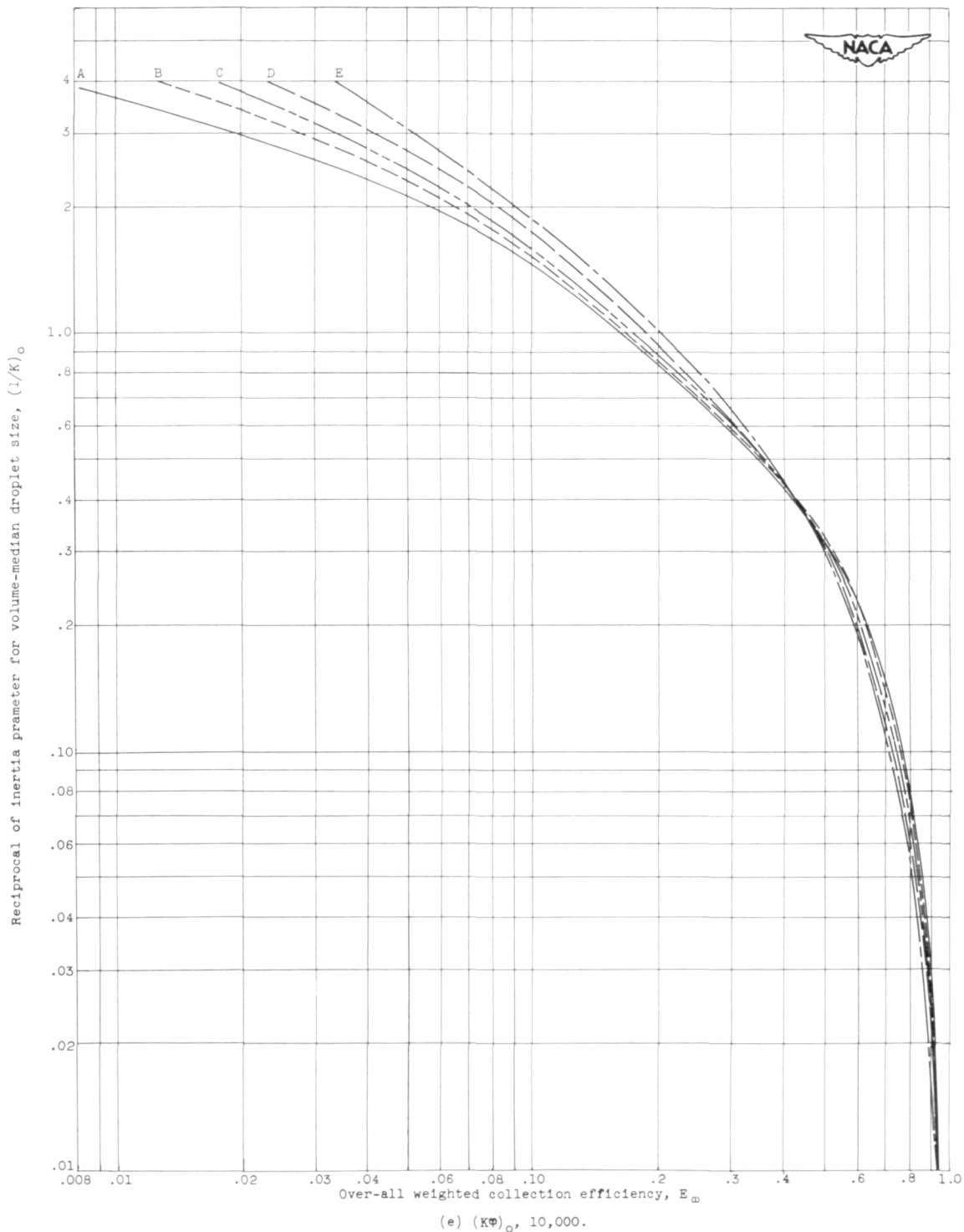


Figure 12. - Concluded. Over-all weighted collection efficiency plotted against reciprocal of inertia parameter for volume-median droplet size for five cloud-droplet-size distributions.

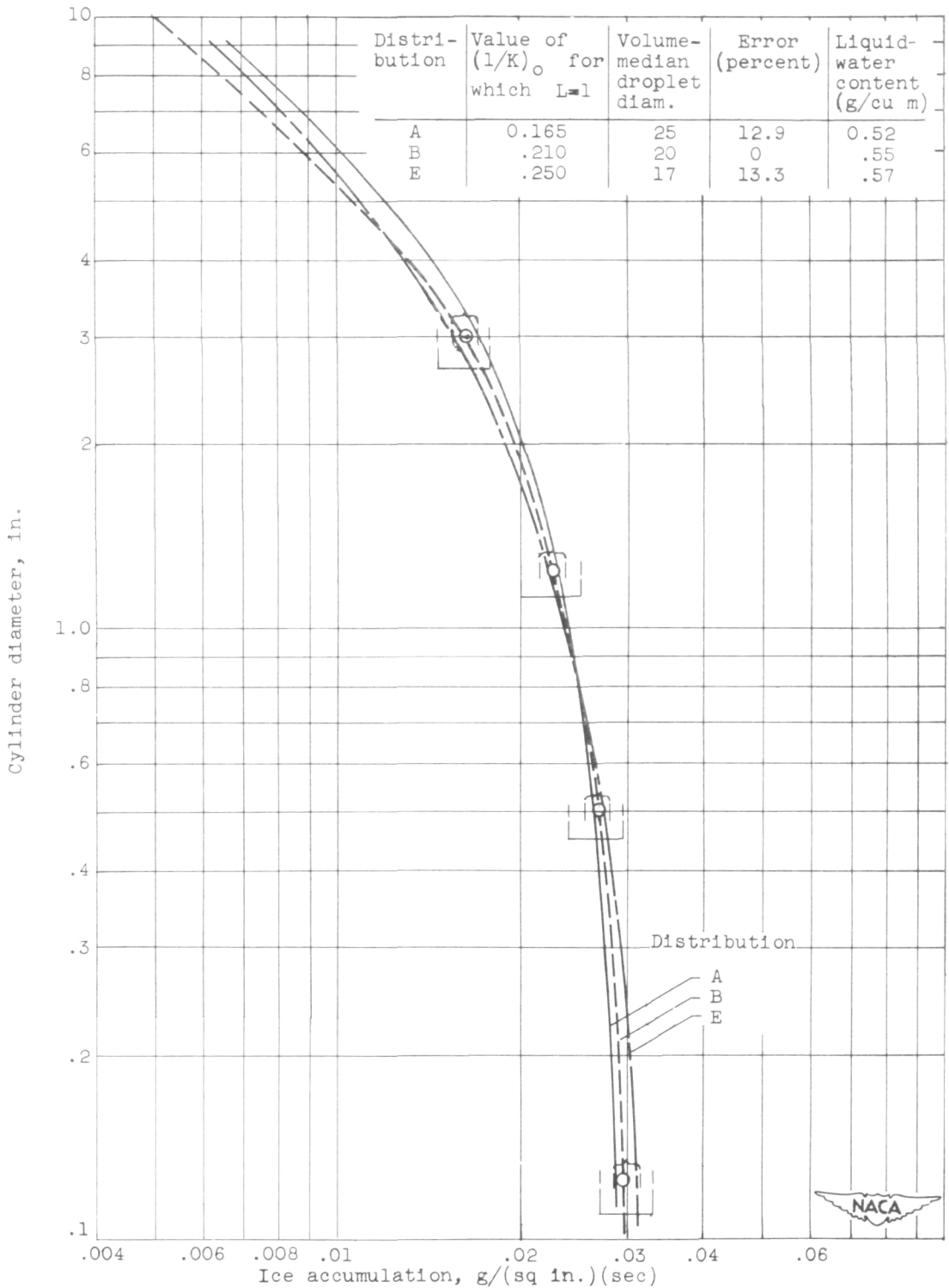
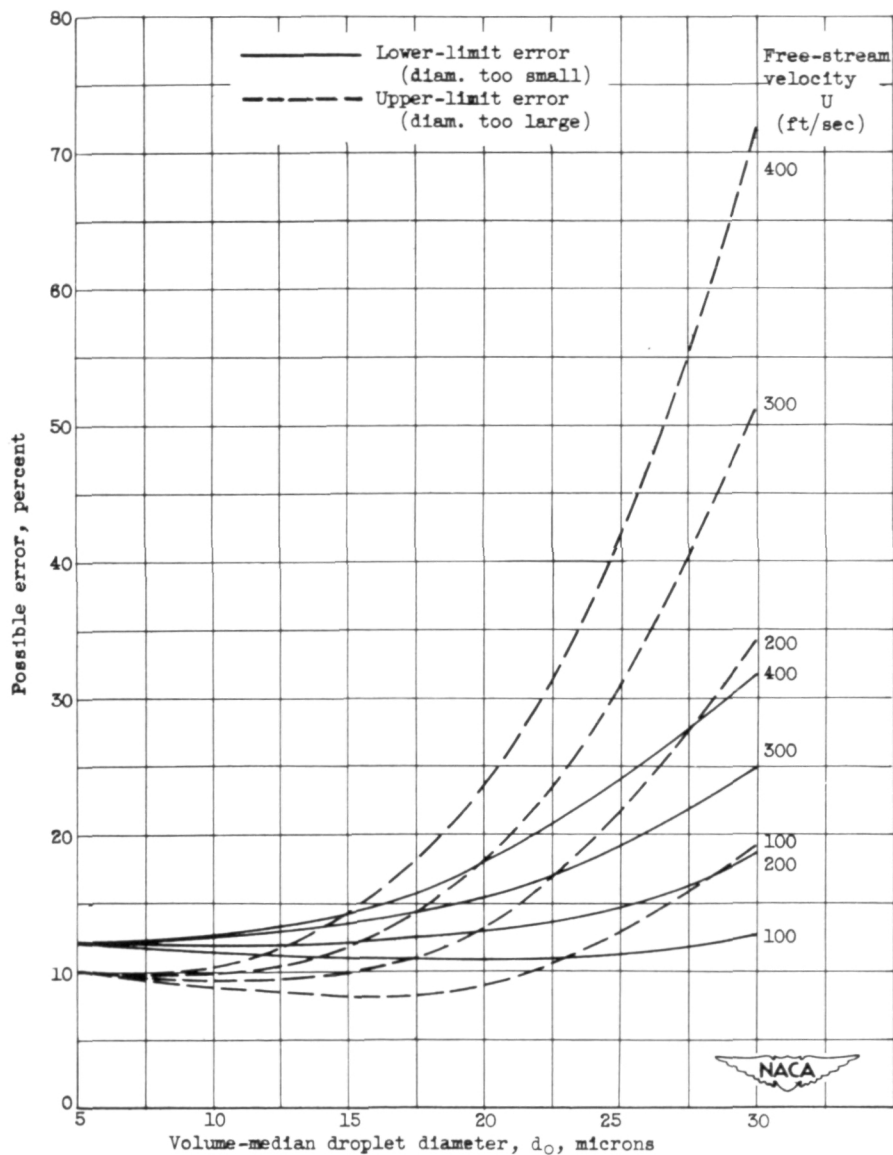
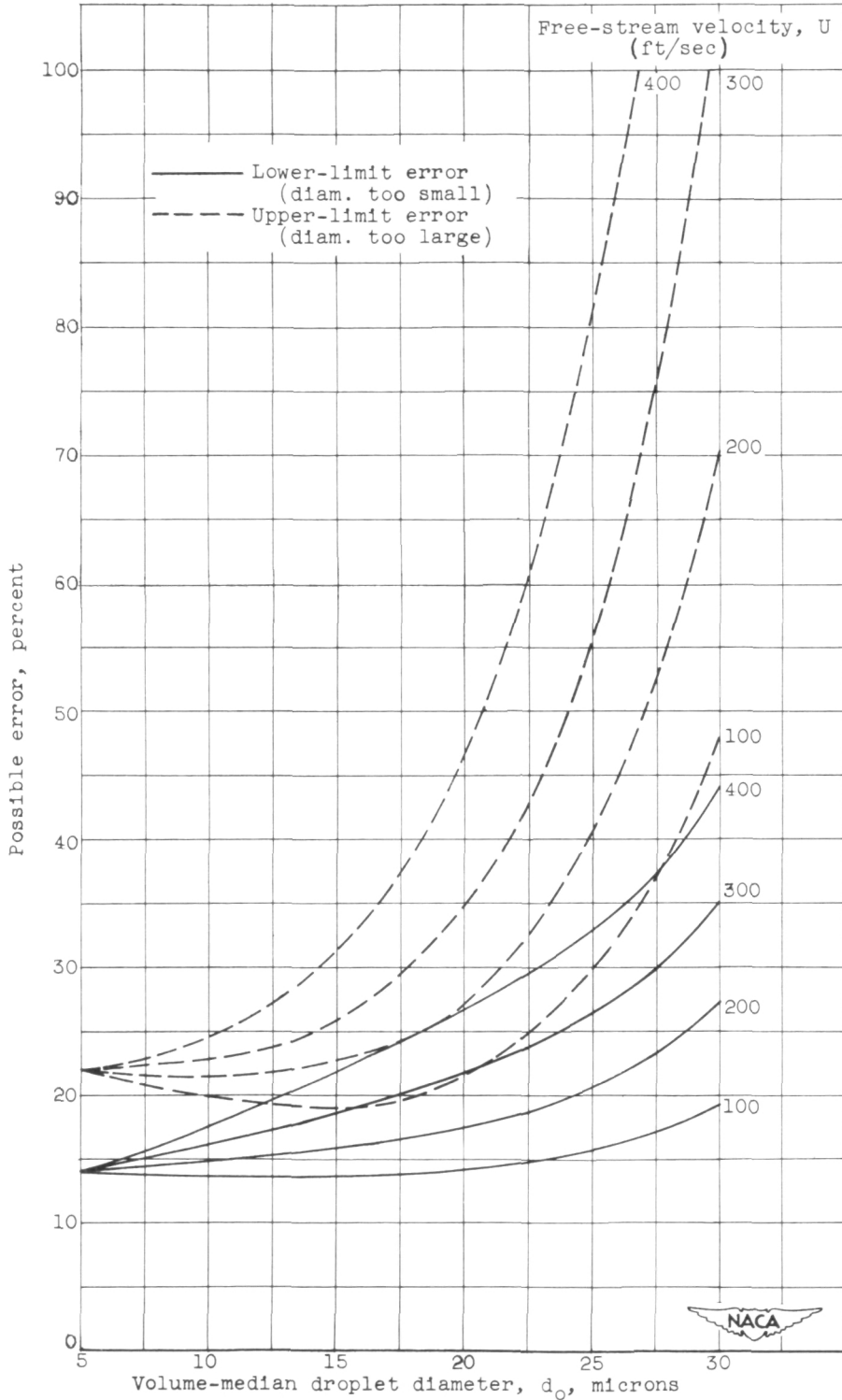


Figure 13. - Comparison of flight data with calculated impingement curves of figure 12(e).  $(K\Phi)_0$ , 10,000. Braces indicate range of  $\pm 5$ -percent error; brackets indicate range of  $\pm 10$ -percent error.



(a) Allowed error in measurement,  $\pm 5$  percent.

Figure 14. - Expected errors in determination of volume-median droplet size.



(b) Allowed error in measurement,  $\pm 10$  percent.

Figure 14. - Concluded. Expected errors in determination of volume-median droplet size.

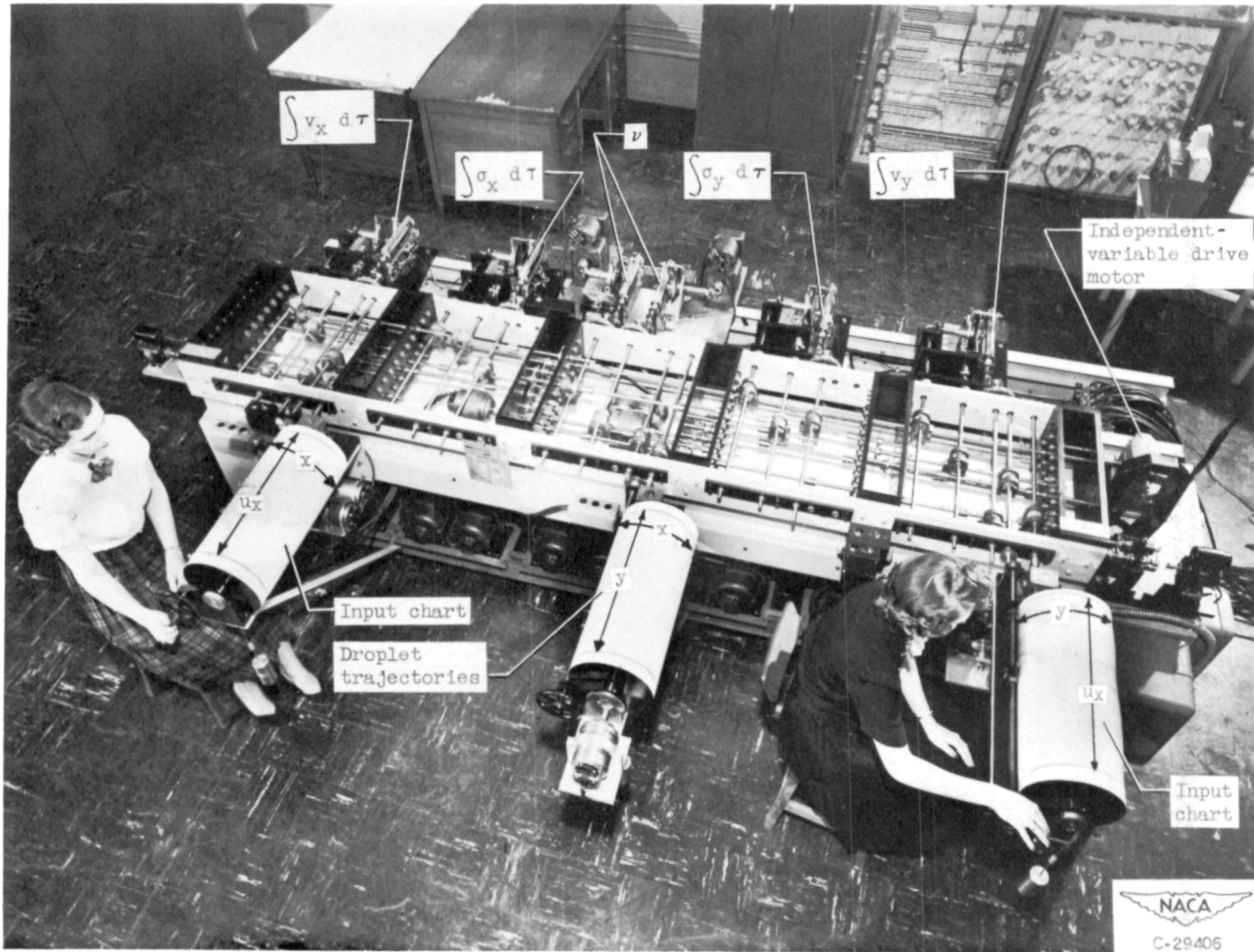


Figure 15. - Water-droplet-trajectory analog.

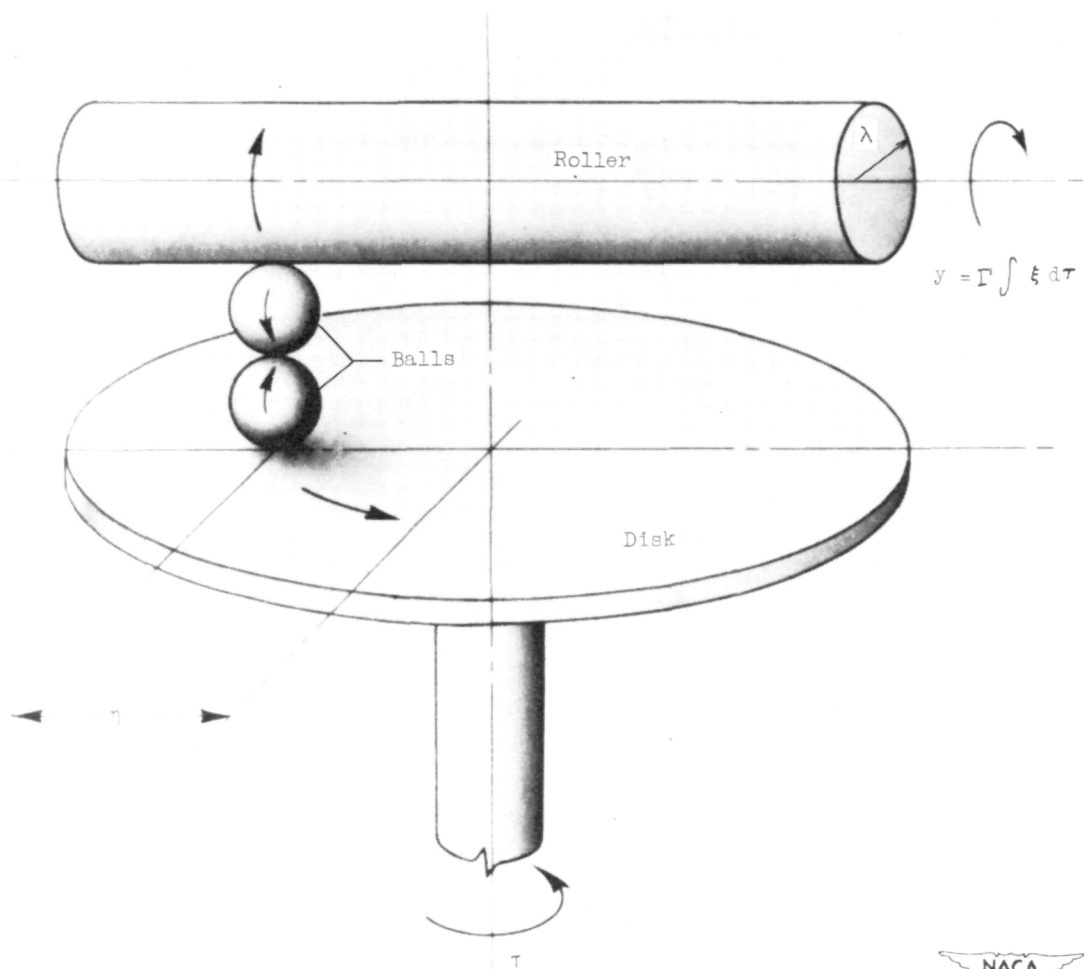


Figure 16. - Principle of integrator.

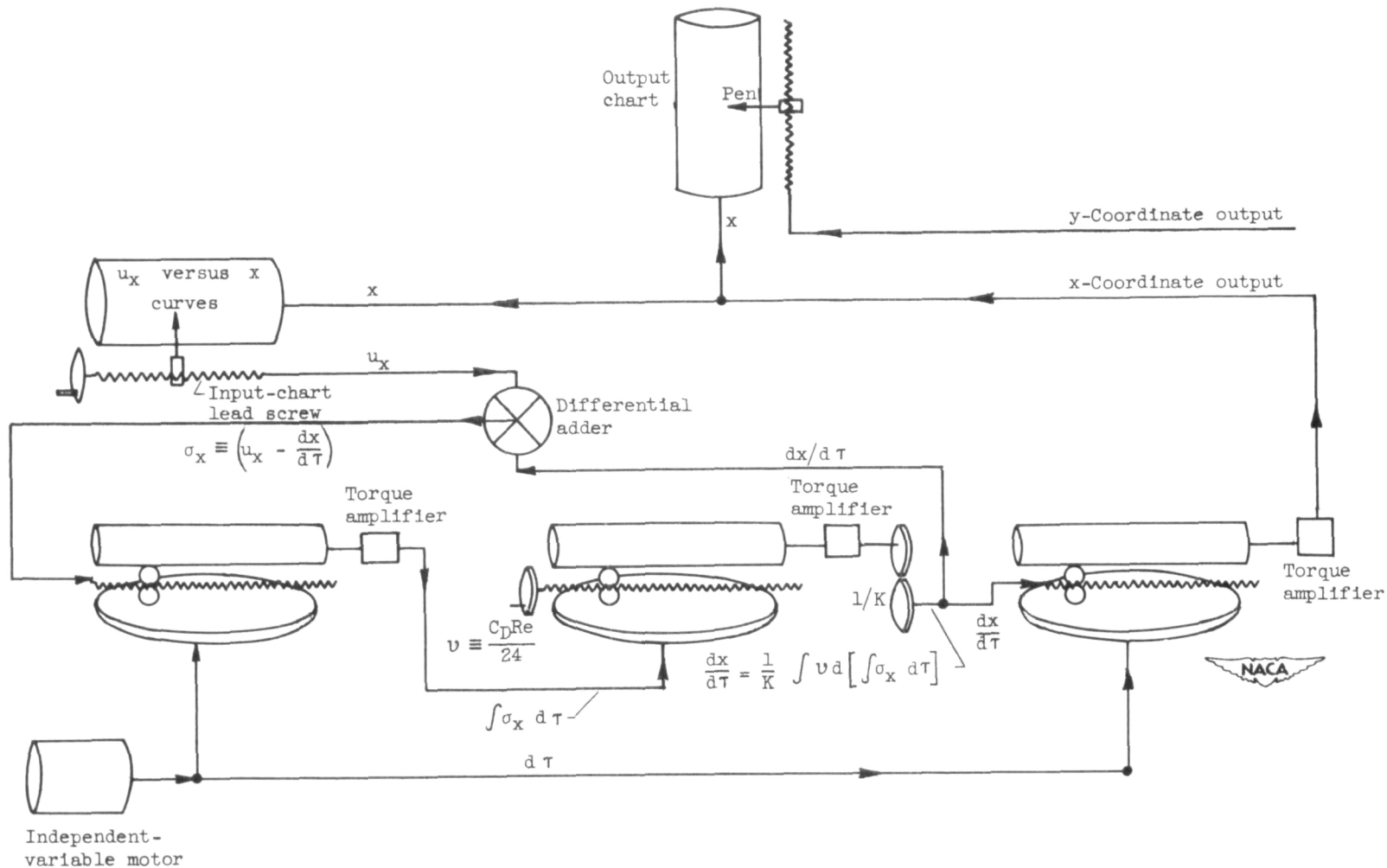
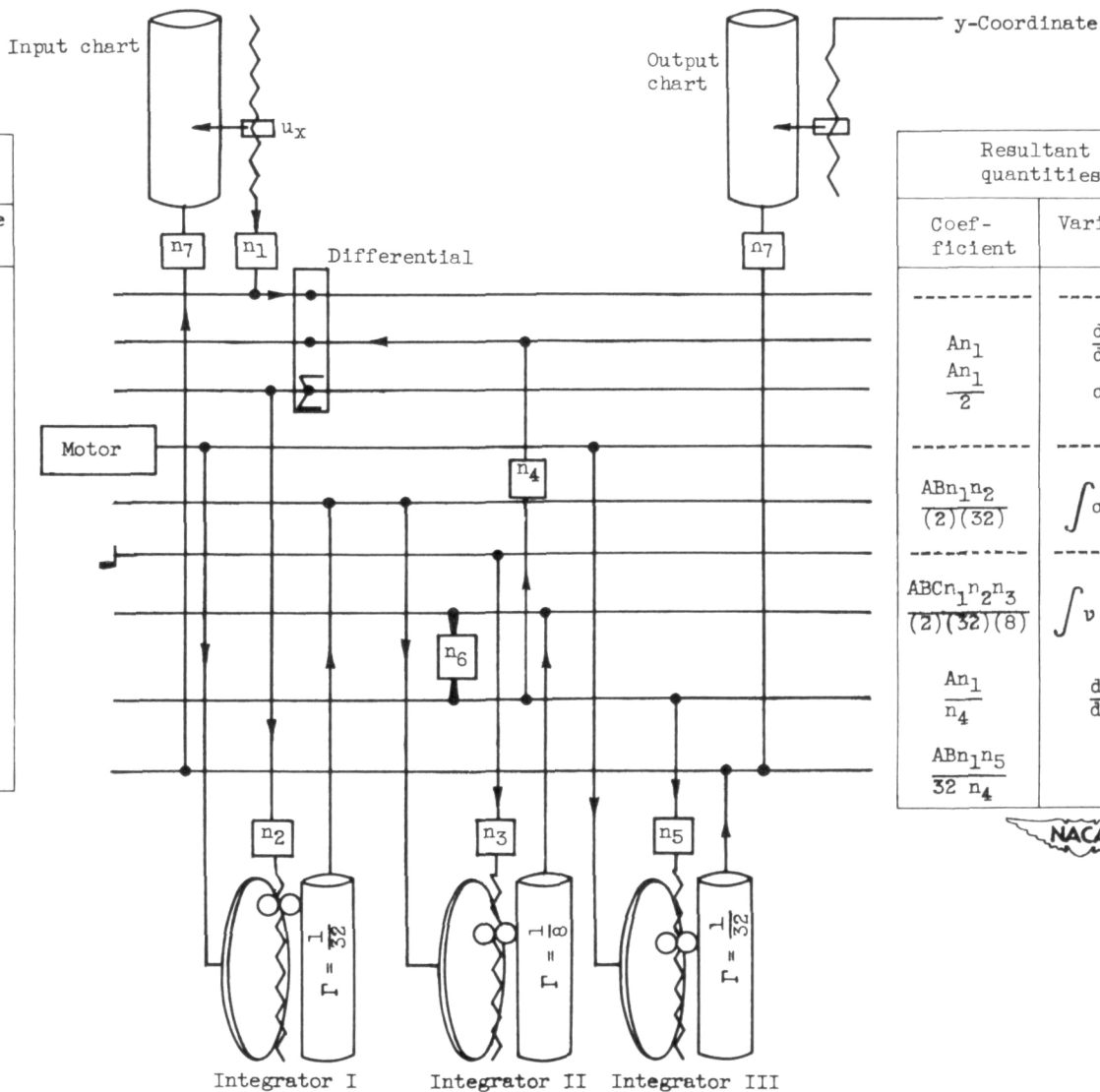


Figure 17. - Computing elements constrained to solve equation  $\frac{dx}{d\tau} = \frac{1}{K} \int \frac{C_D Re}{24} \left( u_x - \frac{dx}{d\tau} \right) d\tau$ . Arrows indicate direction of torque transmission.



Shaft	Intelligence sources	
	Coef-ficient	Variable
1	$An_1$	$u_x$
2	---	--
3	---	--
4	B	$\tau$
5	---	--
6	C	$v$
7	---	--
8	---	---
9	---	--



Resultant quantities	
Coef-ficient	Variable
---	---
$An_1$	$\frac{dx}{d\tau}$
$\frac{An_1}{2}$	$\sigma_x$
---	---
$\frac{ABn_1n_2}{(2)(32)}$	$\int \sigma_x d\tau$
---	---
$\frac{ABCn_1n_2n_3}{(2)(32)(8)}$	$\int v \sigma_x d\tau$
---	---
$\frac{An_1}{n_4}$	$\frac{dx}{d\tau}$
$\frac{ABn_1n_5}{32 n_4}$	$x$



Figure 18. - Schematic diagram used for computing gear ratios.

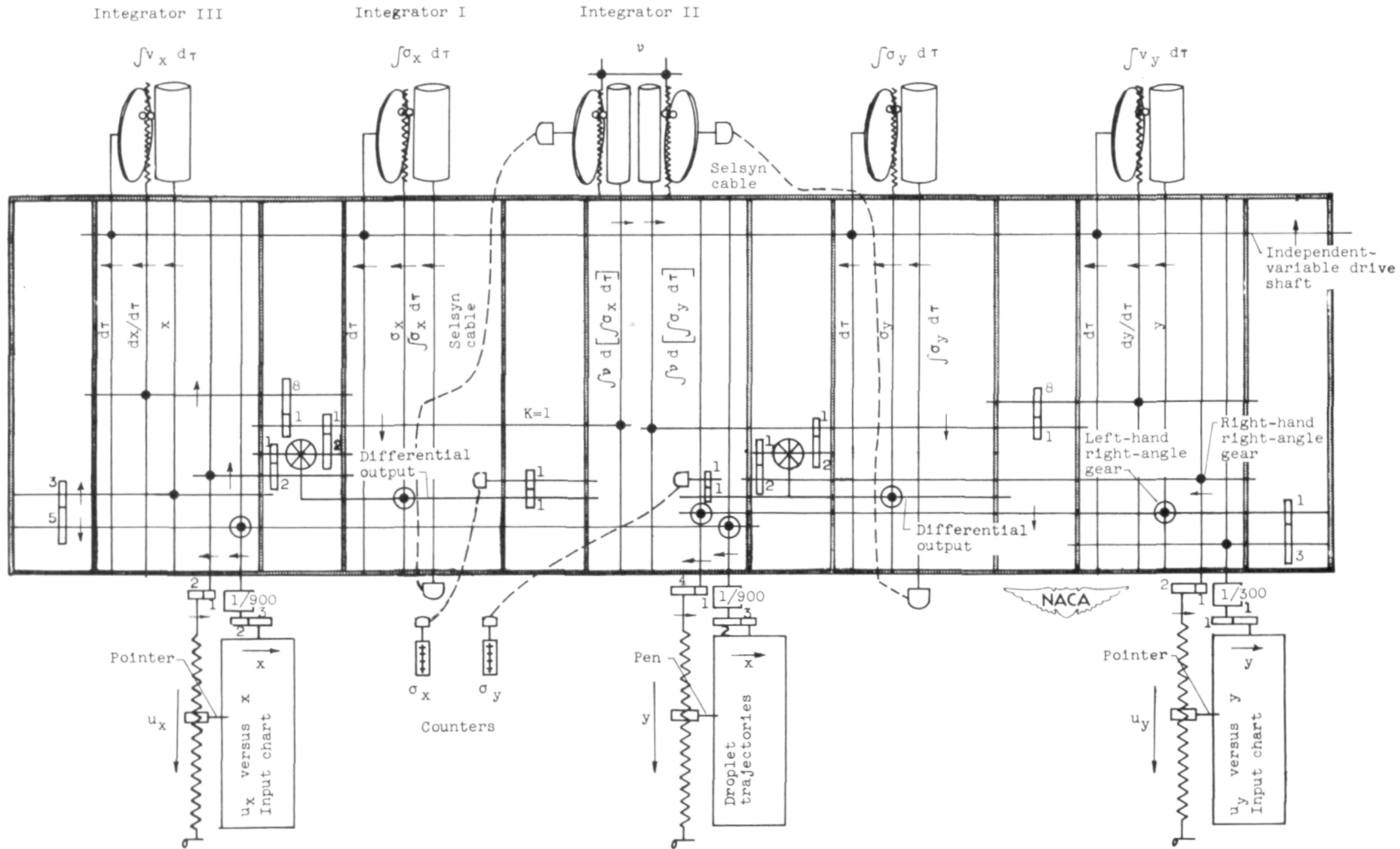


Figure 19. - Plan view of analog setup. Arrows indicate direction of shaft rotation or pen movement for positive sense.